Nonlinear Dyn (2024) 112:3399–3420
https://doi.org/10.1007/s11071-023-09213-z

ORIGINAL PAPER

Parametric reduced-order modeling for component-oriented treatment and localized nonlinear feature inclusion

Konstantinos Vlachas · Anthony Garland · D. Dane Quinn · Eleni Chatzi

Received: 19 May 2023 / Accepted: 11 December 2023 / Published online: 19 January 2024
© The Author(s) 2024

Abstract We propose coupling a physics-based reduction framework with a suited response decomposition technique to derive a component-oriented reduction (COR) approach, which is suitable for assembly systems featuring localized nonlinearities. Dependencies on influencing parameters are injected into the reduced-order model (ROM), thus ensuring robustness and validity over a domain of parametric inputs, while capturing nonlinear effects. The implemented approach employs individual component modes to capture localized features while additionally relying on reduced modes of a global nature to approximate the system's dynamics accurately. The global modes are derived from a linear monolithic system, defined as a result of a coordinate separation scheme, which permits the proposed COR-ROM to naturally couple the response between linear and nonlinear subdomains. The derived low-order representation utilizes a proper orthogonal decomposition projection and is additionally reinforced with the inclusion of a hyper-reduction technique to capture the underlying high-fidelity model response while providing accelerated computations. The resulting approach is exemplified in the synthetic case studies of a four-story shear frame with multiple nonlinear regions driven by hysteresis and a large-scale kingpin connection featuring plasticity.

Keywords Reduced-order models (ROMs) · Component-oriented reduction · Substructuring · Nonlinear dynamics · Virtualization

K. Vlachas (✉) · E. Chatzi
Department of Civil, Environmental, and Geomatic Engineering, ETH Zurich, Stefano-Franscini-Platz 5, Zurich 8093, Switzerland
e-mail: vlachas@ibk.baug.ethz.ch

E. Chatzi
e-mail: chatzi@ibk.baug.ethz.ch

A. Garland
Component Sciences and Mechanics Sandia National Laboratories, Albuquerque, NM, USA
e-mail: agarlan@sandia.gov

D. Quinn
Department of Mechanical Engineering, The University of Akron, Akron, OH, USA
e-mail: quinn@uakron.edu

1 Introduction

Structural and mechanical systems often comprise complex assemblies of multiple components, featuring localized features of elevated intricacy, as present in robotics, automotive, and civil engineering applications [1,2]. This imposes elevated requirements when pursuing a digital twin representation of such systems [3]. The process of twinning is helpful for various tasks, particularly those relating to diagnosis and prognosis, as defined in the Structural Health Monitoring (SHM) or Prognostic Health Management (PHM) context [4,5]. However, evaluating a complex system within a continuous assessment context demands its reduction to ensure affordable numerical computations. To this end, a "divide and conquer" approach is usually

employed, which involves breaking down the system and addressing each component separately [6]. This technique is generally referred to as dynamic substructuring and aims at a component-oriented treatment of the system, meaning that each component is firstly investigated as an individual entity prior to their coupling so as to ultimately re-assemble the global system [7]. The methodological background and the historical development of substructuring methodologies are summarized in [8]. Furthermore, a comparative evaluation of established approaches is provided in [9,10], with more recent techniques exploiting data-driven strategies are discussed in [11–13].

An established technique to achieve high-precision approximations when deriving a digital twin is to imprint the model physics in the virtual representation [14]. In this regard, physics-based reduced-order models (ROMs) refer to low-order numerical representations that additionally retain the real-life system's physical connotation [15]. Essentially, ROMs rely on physics-based reduction to capture the dynamics involved and propagate those in a reduced subspace. This leads to accelerated estimators for downstream tasks, such as decision-making or SHM tasks, which maintain a connection to the underlying physics [16]. Within this context, substructuring can be treated as a tool for injecting component-oriented treatment into the ROMs when addressing complex systems of multiple sub-assemblies [17]. This has been exemplified, for instance, in a linear setting in [18], where a reduced-order model (ROM) for non-classically damped systems is derived relying on the dual Craig-Bampton(CB)-Component Mode Synthesis (CMS) substructuring technique.

Going one step further, the serviceability and utility requirements of a digital twin in SHM applications demand parameterized formulations to address variations in system properties or different operating environments [19,20]. Damage effects have been addressed in [21], where a dual CB-CMS assembly is coupled with Taylor series expansion to address parameterized cracks, whereas interpolation-based strategies on the proper subspace have been proposed instead in [22–25] to derive a linear component-based parametric ROM.

However, the vast majority of the methodologies that are rooted in the principle of dynamic substructuring rely on some form of fundamental modes when attempting to approximate the underlying physics of each component [26,27]. The respective set of modes compresses the response information into a few vectors, which serve as a basis for capturing and efficiently reproducing the original model's complex behavior [28]. Although this simplification straightforwardly holds in a linear setting, localized effects may dominate the response when a system exhibits nonlinearities, thus rendering the conventional treatment ineffective [29,30]. In remedying this deficiency, modal derivatives have been proposed, for example, in [31,32], to augment substructuring representations for geometrically nonlinear systems, while trial vector derivatives have also been reported instead in [33] for structures with nonlinear interfaces.

In that regard, Nonlinear Normal Modes (NNMs) appear as the most referenced strategy for handling localized component nonlinearities [34,35]. In essence, this technique attempts an adaptation of the notion of linear modes employed in the established CMS techniques in a nonlinear setting [36]. Computational approaches for NNMs extraction have been proposed in [37–40], whereas the notion of (complex) NNMs has already been proven effective in a variety of applications, including resonance prediction [41], frequency response approximation [42], or nonlinear friction modeling [43]. More recently, Joannin et al. [44] coupled a NNMs-based strategy with modal synthesis to address vibration applications in large Finite Element (FE) models, thus providing more general applicability.

However, despite recent efforts, the available frameworks for determining the NNMs seem to remain computationally intensive, problem-specific, or limited to models with a relatively small dimension. In addition, the respective NNMs-based approaches do not allow for constructing a forward model that propagates the dynamics in time, thus relying on ad-hoc, data-driven schemes for such tasks. The Proper Orthogonal Decomposition (POD) poses a compromising yet computationally tractable and generally applicable alternative that can additionally be utilized to formulate a forward ROM via the use of projection techniques. A set of modes is derived by applying POD in a series of response time histories, which has been shown to deliver a sufficiently accurate approximation of the actual NNMs [45]. More importantly, though, the POD projects the dynamics in a low-order subspace that additionally allows for direct integration. Thus, POD-based ROMs require no additional technique to evaluate the model response forward in time, contrary to

frameworks relying on the extraction of NNMs, which typically require a data-driven temporal mapping, as for example the LSTM neural networks suggested in [46].

In this work, we propose a physics-based, component-oriented ROM, termed as Component-Oriented Reduction (COR)-ROM. Through POD-based projection, the derived representation can address parametrically-dependent, nonlinear systems and capture response information on a global system scale and on a localized level. To achieve this, the ROM assembly presented in [47] is recast into a substructural formulation based on the decomposition proposed in [48] to enable individual treatment of each component during reduction while incorporating localized nonlinear features. This decomposition has already been used in [49] to derive a global, system-wide ROM approach using modal reduction while evaluating the localized features in full order, whereas in [50] the decomposition is utilized in a machine learning framework for identification of interface forcing.

Moreover, coupling POD for the system-wide reduction with a CMS-based formulation for substructuring has already been explored in [51–53]. However, the linear nature of the CMS modes utilized poses certain limitations regarding capturing nonlinear effects on a component level. In addition, such approaches address nonlinear systems with a ROM that relies on a single global projection basis. This implies limited applicability as only a limited range of configurations can be captured, or the number of required modes will make the basis intractable [54].

Further, a powerful trait of the adopted COR-ROM strategy is revealed within the reduction context. By properly decomposing the response into a linear portion resulting from the monolithic assembly of the system and a deviatoric one, which captures the nonlinear effects, the proposed scheme feeds the COR-ROM with response information on both a global (system) and a localized (component) level. This technique further extends CMS-based strategies that rely solely on the latter. The COR-ROM reduced-order basis, on the one hand, allows for the use of system-wide reduction that captures the global modes, i.e., the modes that represent the dynamics of a linear monolithic assembly, in the absence of localized nonlinear effects. On the other hand, the localized features are assembled in a component-wise manner into the ROM via POD reduction onto the nonlinear (deviatoric) portion of the response. This approach allows for the adoption of any reduced-order basis projection technique, while enabling the potential of hyper-accelerated ROMs using second-tier approximations like hyper-reduction. The latter allows the ROM to project and evaluate the nonlinear terms in a reduced subspace, thus achieving additional efficiency [55–57].

The proposed framework further tackles the necessity of adaptive exploration of the input sampling domain during the full-order evaluations of the training phase. A sampling technique with a suitable error indicator is utilized for this purpose, following relevant suggestions in [58]. Similar to previous works in [59,60], the Modal Assurance Criterion (MAC) is employed as a comparative measure that indirectly relates the underlying dynamics of neighboring parametric samples as captured by the projection bases.

The efficacy of the derived COR-ROM is illustrated in a numerical benchmark of a four-story shear frame with multiple nonlinear domains driven by hysteretic nodal connections [61,62], and in a three-dimensional kingpin case study featuring material plasticity. The latter large-case example further demonstrates the ability of the ROM to reduce the required computational toll and offer accelerated model evaluations for complex structures.

The remainder of the paper is structured as follows. In Sect. 2, the problem statement is offered. The main components of the proposed framework are presented in detail in Sect. 3 and Sect. 4, where the implemented substructuring approach and the parametric reduced-order modeling framework details are clarified, respectively. In Sect. 5, the various aspects of the ROM performance are evaluated through a series of numerical experiments. Finally, Sect. 6 summarizes the main results and discusses the potential and limitations of the proposed framework.

2 Problem statement

The general problem setting of our work is the physics-based, component-oriented reduction of parameterized dynamical systems comprising assemblies of components with localized features, which impact the overall dynamics. Such localized effects may correspond to the manifestation of damage and/or local deterioration or might arise from the inherent composition of the system, which can include joints, interfaces, or non-

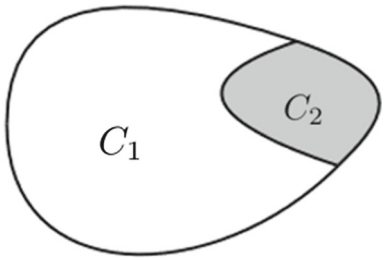

Fig. 1 Abstraction of a nonlinear instance, which is assumed localized within the region C_2, within an otherwise linear domain C_1 (illustration adjusted from [49])

linear attachments. For the sake of demonstration, and without compromising the potential generalization of our work, we assume a problem setting pertaining to the presence of a localized nonlinearity, which is activated only within a region of the general system under consideration, as illustrated in Fig. 1. The general case, where multiple regions of nonlinearity are present, can be tackled similarly, since the proposed approach does not assume any physical connectivity. It, instead, solely relies on a coordinates-based partitioning of the equations of motion, as described next. Thus, Fig. 1 is an example illustration of one such instance. In Sect. 5, a numerical case study featuring two nonlinear domains is also explored for the sake of completeness.

Regarding the mathematical description, we first assume a nonlinear dynamical system additionally conditioned on a parameter vector $\boldsymbol{\mu} = [\mu_1, \ldots, \mu_{N_p}] \in \mathbb{R}^{N_p}$, which captures all system properties and excitation-relevant traits. The dynamic motion is thus described by the following set of nonlinear governing equations:

$$\boldsymbol{M}\ddot{\boldsymbol{u}}(t) + \boldsymbol{g}\left(\boldsymbol{u}(t), \dot{\boldsymbol{u}}(t), \boldsymbol{\mu}\right) = \boldsymbol{f}(t, \boldsymbol{\mu}) \tag{1}$$

where $\boldsymbol{u}(t) \in \mathbb{R}^N$ represents the system's behavior in terms of displacements, $\boldsymbol{M} \in \mathbb{R}^{N\times N}$ represents the mass matrix, and $\boldsymbol{f}(t, \boldsymbol{\mu}) \in \mathbb{R}^n$ the external excitation. Variable N expresses the order of the system, which denotes the dimensionality of the coordinate space and physically represents the number of Degrees Of Freedom (DOFs) in the system. Lastly, the restoring force term $\boldsymbol{g}\left(\boldsymbol{u}(t), \dot{\boldsymbol{u}}(t), \boldsymbol{\mu}\right) \in \mathbb{R}^N$ models the nonlinear effects, encoding phenomena that range from material nonlinearity to hysteresis or interface nonlinearities.

Since we are dealing with a dynamic problem, the respective governing equations in Eq. (1) are to be solved incrementally by means of time discretization and numerical integration. Thus, the equations of motion and any equilibrium conditions are typically linearized about the current configuration prior to proceeding with the computation of the quantities required for the next time increment. The tangent stiffness matrix naturally appears during this procedure. As a result, the respective linearized form of the governing equations at iteration gives:

$$\boldsymbol{g}\left(\delta\boldsymbol{u}, \boldsymbol{\mu}\right) = \tilde{\boldsymbol{K}}(\delta\boldsymbol{u}, \boldsymbol{\mu})\delta\boldsymbol{u} + \boldsymbol{G}_\star\left(\delta\boldsymbol{u}, \boldsymbol{\mu}\right) \tag{2}$$

where time dependency has been dropped, $\tilde{\boldsymbol{K}} \in \mathbb{R}^{N\times N}$ denotes the tangent stiffness matrix, $\delta\boldsymbol{u}$ is the incremental displacement, and the term $\boldsymbol{G}_\star\left(\delta\boldsymbol{u}, \boldsymbol{\mu}\right)$ represents the vector assembly of the (remaining) nonlinear terms in the system. Without compromising the applicability, the setup further assumes linear damping forces, so the dependency in $\dot{\boldsymbol{u}}$ has been omitted for simplicity.

We now decompose our structure, which is illustrated in Fig. 1, into two adjacent regions, denoted by C_1 and C_2, respectively. This decomposition assumes that any nonlinearities are localized within C_2, while the behavior within C_1 remains linear. In this setting, region C_1 is described by the internal variables $\boldsymbol{u_1} \in \mathbb{R}^{N_1}$, while $\boldsymbol{u_2} \in \mathbb{R}^{N_2}$ are the corresponding internal variables for C_2. As a result, the following holds:

$$\begin{aligned} \boldsymbol{G}_\star = [\boldsymbol{0} \quad \boldsymbol{G}(\delta\boldsymbol{u_2}, \boldsymbol{\mu})]^{\mathrm{T}} \in \mathbb{R}^{N=(N_1+N_2)}, \quad \mathbf{G} \in \mathbb{R}^{N_2} \\ \delta\boldsymbol{u} = [\delta\boldsymbol{u_1} \quad \delta\boldsymbol{u_2}]^{\mathrm{T}} \in \mathbb{R}^{N=(N_1+N_2)} \end{aligned} \tag{3}$$

Thus, the term $\boldsymbol{G}$ represents the nonlinearities localized in the region C_2, whereas the parametric traits $\boldsymbol{\mu}$ also influence the update process of the system matrices, especially the reconstruction of the tangent stiffness matrix. Hereafter, our description refers to the linearized form of Eq. (1).

At this point, we additionally assume that within the linear region C_1, the physical coordinates can be expressed as $\delta\boldsymbol{u_1} = [\delta\boldsymbol{u}_c \quad \delta\boldsymbol{u}_\alpha]^{\mathrm{T}}$, where $\boldsymbol{u}_\alpha$ represents the vector of those DOFs that are coupled to the isolated region C_2. Likewise, within C_2 the coordinates that are coupled to C_1 can be identified as $\boldsymbol{u}_\beta$, so that $\delta\boldsymbol{u_2} = \left[\delta\boldsymbol{u}_\beta \quad \delta\boldsymbol{u}_n\right]^{\mathrm{T}}$. Thus, the terms in Eqs. (1) and (2) can be rewritten as:

$$\boldsymbol{M} = \begin{bmatrix} \boldsymbol{M}_{cc} & \boldsymbol{M}_{c\alpha} & \boldsymbol{0} & \boldsymbol{0} \\ \boldsymbol{M}_{c\alpha}^{\mathrm{T}} & \boldsymbol{M}_{\alpha\alpha} & \boldsymbol{M}_{\alpha\beta} & \boldsymbol{0} \\ \boldsymbol{0} & \boldsymbol{M}_{\alpha\beta}^{\mathrm{T}} & \boldsymbol{M}_{\beta\beta} & \boldsymbol{M}_{\beta n} \\ \boldsymbol{0} & \boldsymbol{0} & \boldsymbol{M}_{\beta \mathrm{n}}^{\mathrm{T}} & \boldsymbol{M}_{nn} \end{bmatrix}$$

$$\tilde{\boldsymbol{K}} = \begin{bmatrix} \tilde{\boldsymbol{K}}_{cc} & \tilde{\boldsymbol{K}}_{c\alpha} & \boldsymbol{0} & \boldsymbol{0} \\ \tilde{\boldsymbol{K}}_{c\alpha}^{\mathrm{T}} & \tilde{\boldsymbol{K}}_{\alpha\alpha} & \tilde{\boldsymbol{K}}_{\alpha\beta} & \boldsymbol{0} \\ \boldsymbol{0} & \tilde{\boldsymbol{K}}_{\alpha\beta}^{\mathrm{T}} & \tilde{\boldsymbol{K}}_{\beta\beta} & \tilde{\boldsymbol{K}}_{\beta n} \\ \boldsymbol{0} & \boldsymbol{0} & \tilde{\boldsymbol{K}}_{\beta \mathrm{n}}^{\mathrm{T}} & \tilde{\boldsymbol{K}}_{nn} \end{bmatrix}$$

$$\delta \boldsymbol{u} = \begin{bmatrix} \delta \boldsymbol{u}_c \\ \delta \boldsymbol{u}_\alpha \\ \delta \boldsymbol{u}_\beta \\ \delta \boldsymbol{u}_n \end{bmatrix}, \boldsymbol{G}_\star = \begin{bmatrix} \boldsymbol{0} \\ \boldsymbol{0} \\ \boldsymbol{G}_\beta \\ \boldsymbol{G}_n \end{bmatrix}, \delta \boldsymbol{f} = \begin{bmatrix} \delta \boldsymbol{f}_c \\ \delta \boldsymbol{f}_\alpha \\ \delta \boldsymbol{f}_\beta \\ \delta \boldsymbol{f}_n \end{bmatrix} \tag{4}$$

where $\delta \boldsymbol{u}_\alpha \in \mathbb{R}^{N_\alpha}, \delta \boldsymbol{u}_c \in \mathbb{R}^{N_c}, \delta \boldsymbol{u}_\beta \in \mathbb{R}^{N_\beta}, \delta \boldsymbol{u}_n \in \mathbb{R}^{N_n}$ with $N_c \gg N_n > (N_\alpha, N_\beta)$, and the subscripts denote the DOFs for the corresponding block sub-matrices. In addition, in the presence of nonlinear damping forces, the damping matrix $\boldsymbol{C} \in \mathbb{R}^{N \times N}$ can be decomposed, and Eq. (2) can be adjusted accordingly. As already explained, the above scheme relies solely on a partitioning strategy. Thus, in the presence of multiple nonlinear features represented by several distinct isolated regions, the respective block matrices that correspond to the relevant DOFs of the regions may be uncoupled in the $\boldsymbol{M}_n$, $\tilde{\boldsymbol{K}}_n$ matrices and additional block matrices would be needed for the interface DOFs.

3 Component-oriented treatment

The response $\boldsymbol{u_2}$ of the isolated region C_2 in Fig. 1 is dominated by the presence of localized (nonlinear or damage) effects. Based on the approach proposed in [49], we assume the following decomposition: $\delta \boldsymbol{u_2} = \delta \boldsymbol{x} + \delta \boldsymbol{z}$, where $\boldsymbol{x}$ represents an idealized system to be subsequently defined, and $\boldsymbol{z}$ functions as a deviatoric component, which captures the residual response between the idealized and the actual configuration. Based on Eq. (4), the decomposition implies that the deviatoric response $\delta \boldsymbol{z}$ is driven by the terms $\boldsymbol{G}$ representing the nonlinear forcing due to the features in C_2. In addition, as the linear region C_1 only experiences global idealized features, the global response vector of the system can now be expressed as $\delta \boldsymbol{u} = \begin{bmatrix} \delta \boldsymbol{u}_c & \delta \boldsymbol{u}_\alpha & \delta \boldsymbol{x}_\beta & \delta \boldsymbol{x}_n \end{bmatrix}^{\mathrm{T}} + \begin{bmatrix} \boldsymbol{0} & \boldsymbol{0} & \delta \boldsymbol{z}_\beta & \delta \boldsymbol{z}_n \end{bmatrix}^{\mathrm{T}}$. With these definitions in place, the term $\tilde{\boldsymbol{K}} \delta \boldsymbol{u}$ in Eq. (2) for example can be rewritten as:

$$\begin{aligned} \tilde{\boldsymbol{K}} \delta \boldsymbol{u} &= \tilde{\boldsymbol{K}} \begin{bmatrix} \delta \boldsymbol{u}_c \\ \delta \boldsymbol{u}_\alpha \\ \delta \boldsymbol{x}_\beta + \delta \boldsymbol{z}_\beta \\ \delta \boldsymbol{x}_n + \delta \boldsymbol{z}_n \end{bmatrix} \\ &= \tilde{\boldsymbol{K}} \delta \boldsymbol{w} + \begin{bmatrix} \boldsymbol{0}_c \\ \tilde{\boldsymbol{K}}_{\alpha\beta} \delta \boldsymbol{z}_\beta \\ \boldsymbol{0}_2 \end{bmatrix} + \begin{bmatrix} \boldsymbol{0}_c \\ \boldsymbol{0}_\alpha \\ \tilde{\boldsymbol{K}}_2 \delta \boldsymbol{z} \end{bmatrix} \end{aligned} \tag{5}$$

where,

$$\begin{aligned} \tilde{\boldsymbol{K}}_2 &= \begin{bmatrix} \tilde{\boldsymbol{K}}_{\beta\beta} & \tilde{\boldsymbol{K}}_{\beta n} \\ \tilde{\boldsymbol{K}}_{\beta n}^{\mathrm{T}} & \tilde{\boldsymbol{K}}_{nn} \end{bmatrix} \in \mathbb{R}^{N_2}, \\ \delta \boldsymbol{z} &= \begin{bmatrix} \delta \boldsymbol{z}_\beta & \delta \boldsymbol{z}_n \end{bmatrix}^{\mathrm{T}} \in \mathbb{R}^{N_n} \end{aligned} \tag{6}$$

and the sub-indices in $\boldsymbol{0}_c$ indicate the dimensionality of the null vector, e.g., $\boldsymbol{0}_c \in \mathbb{R}^{N_c}$. Here, the coupling term $\tilde{\boldsymbol{K}}_{\alpha\beta} \delta \boldsymbol{z}_\beta$ acts on the coupling DOFs associated with $\boldsymbol{u}_\alpha$, while the respective elastic term $\tilde{\boldsymbol{K}}_{\alpha\beta}^{\mathrm{T}} \delta \boldsymbol{u}_\alpha$ is included in the term $\tilde{\boldsymbol{K}} \delta \boldsymbol{w} \in \mathbb{R}^N$.

The mixed displacement vector $\delta \boldsymbol{w}$ is defined as:

$$\delta \boldsymbol{w} = \begin{bmatrix} \delta \boldsymbol{u}_c & \delta \boldsymbol{u}_\alpha & \delta \boldsymbol{x}_\beta & \delta \boldsymbol{x}_n \end{bmatrix}^{\mathrm{T}} = \begin{bmatrix} \delta \boldsymbol{u}_1 & \delta \boldsymbol{x} \end{bmatrix}^{\mathrm{T}} \tag{7}$$

Thus, $\delta \boldsymbol{u_1}$ represents the response in the exterior region C_1 exactly, while $\delta \boldsymbol{x}$ is the respective idealized response in the isolated domain C_2. As a result, the system as expressed in Eqs. (1) and (2) can be reformulated using Eq. (5) and applying the same transformation in $\boldsymbol{M}$. The resulting (linearized) system reads:

$$\begin{aligned} &\boldsymbol{M} \delta \ddot{\boldsymbol{w}} + \begin{bmatrix} \boldsymbol{0}_c \\ \boldsymbol{M}_{\alpha\beta} \delta \ddot{\boldsymbol{z}}_\beta \\ \boldsymbol{0}_2 \end{bmatrix} + \begin{bmatrix} \boldsymbol{0}_c \\ \boldsymbol{0}_\alpha \\ \boldsymbol{M}_2 \delta \ddot{\boldsymbol{z}} \end{bmatrix} \\ &\quad + \tilde{\boldsymbol{K}} \delta \boldsymbol{w} + \begin{bmatrix} \boldsymbol{0}_c \\ \tilde{\boldsymbol{K}}_{\alpha\beta} \delta \boldsymbol{z}_\beta \\ \boldsymbol{0}_2 \end{bmatrix} + \begin{bmatrix} \boldsymbol{0}_c \\ \boldsymbol{0}_\alpha \\ \tilde{\boldsymbol{K}}_2 \delta \boldsymbol{z} \end{bmatrix} \\ &\quad + \begin{bmatrix} \boldsymbol{0}_c \\ \boldsymbol{0}_\alpha \\ \boldsymbol{G}(\delta \boldsymbol{x} + \delta \boldsymbol{z}) \end{bmatrix} = \delta \boldsymbol{f} \end{aligned} \tag{8}$$

where dependencies have been dropped, and

$$\begin{aligned} &\boldsymbol{G}(\delta \boldsymbol{x} + \delta \boldsymbol{z}) \\ &\qquad = \begin{bmatrix} \boldsymbol{G}(\delta \boldsymbol{x}_\beta + \delta \boldsymbol{z}_\beta)^{\mathrm{T}} & \boldsymbol{G}(\delta \boldsymbol{x}_n + \delta \boldsymbol{z}_n)^{\mathrm{T}} \end{bmatrix}^{\mathrm{T}} \end{aligned} \tag{9}$$

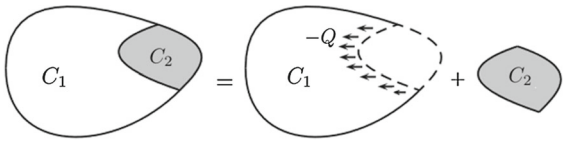

Fig. 2 Schematic of the decomposition of the isolated region C_2 (illustration adjusted from [49])

and the matrix $\boldsymbol{M}_2$ is assembled similarly to $\tilde{\boldsymbol{K}}_2$ in Eq. (6). Therefore, Eq. (8) implies that the dynamic response of the system may be represented in an exact manner in the exterior region C_1, but the deviatoric component $\delta \boldsymbol{z}$ is required. By further partitioning Eq. (8) we can derive the following two separate (linearized) systems of governing equations in terms of the mixed variable $\delta \boldsymbol{w}$ and the deviatoric one $\delta \boldsymbol{z}$:

$$\boldsymbol{M}\delta\ddot{\boldsymbol{w}} + \tilde{\boldsymbol{K}}\delta\boldsymbol{w} = \delta\boldsymbol{f} - \delta\boldsymbol{Q} \tag{10}$$

$$\boldsymbol{M}_2\delta\ddot{\boldsymbol{z}} + \tilde{\boldsymbol{K}}_2\delta\boldsymbol{z} + \boldsymbol{G}(\delta\boldsymbol{x} + \delta\boldsymbol{z}) = \boldsymbol{0} \tag{11}$$

with,

$$\delta\boldsymbol{Q} = \begin{bmatrix}\boldsymbol{0}_c & \delta\boldsymbol{Q}_\star & \boldsymbol{0}_2\end{bmatrix}^{\mathrm{T}} \in \mathbb{R}^{N=(N_c+N_a+N_2)}$$

$$\delta\boldsymbol{Q}_\star \equiv \left(\boldsymbol{M}_{\alpha\beta}\delta\ddot{\boldsymbol{z}}_\beta + \tilde{\boldsymbol{K}}_{\alpha\beta}\delta\boldsymbol{z}_\beta\right) \tag{12}$$

Thus, in Eq. (11), the deviatoric response $\delta \boldsymbol{z}$ in the isolated region C_2 is driven by the idealized system represented by the response vector $\delta \boldsymbol{x}$ through the nonlinear effects. In parallel, region C_1 is linearly coupled to the deviatoric response $\delta \boldsymbol{z}$ through the force term $\delta \boldsymbol{Q}$.

As a result, the mixed formulation with respect to $\delta \boldsymbol{w}$ on the first set of equations in Eq. (10) is linear, while the nonlinear behavior is retained within the isolated region through Eq. (11). A schematic representation of this substructuring-inspired decomposition is presented in Fig. 2.

The above set of Eqs. (10) and (11) also comprises the governing equations for the linearized version of the full-order model (FOM) employed herein, with the goal being to derive a ROM for accelerated approximations. The demonstrated scheme enables a substructuring-based treatment of the problem at hand in a ROM level, as the low-order representation can now harvest response information in a twofold manner: both on a global system scale via Eq. (10) and on a localized level where nonlinear features exist via Eq. (11). This enables a component-oriented reduction to subsequently derive a COR-ROM, which replicates the global system behavior while accurately capturing localized features concentrated in a region of the system.

4 Assembly of the COR-ROM

Several alternatives exist for constructing efficient reduced-order representations for the problem at hand, as described in Sect. 2. In this work, we employ a Galerkin projection-based scheme since a projection-based approach allows for a low-order representation of the full physical space of the model. This implies that we simultaneously capture displacements, strains, stresses, and accelerations and further relevant physical or energy measures. This is beneficial with respect to the alternate approach of deriving a ROM for specific elements or only a few sparse nodes [27]. In addition, this ability of the ROM to capture the full space of the high-fidelity response potentially increases, to a certain extent, its utility for generalized response prediction or parameter estimation tasks, thus featuring as a component of a higher level SHM system [54]. Herein, the ROM framework is described. Our methodology assumes the availability of a high fidelity FOM, in our case a FE model, functioning as the spatially discretized full-order representation of the system in Eqs. (10) and (11).

4.1 Projection-based model-order reduction

Projection-based ROMs rely on the assumption that the dynamic response $\boldsymbol{u}$ lies in a subspace of size r, where r is much smaller than the physical dimensionality of the original problem ($r \ll N$). Thus, the following holds:

$$\boldsymbol{u}(t) \approx \boldsymbol{V}(\boldsymbol{\mu})\,\boldsymbol{y}(t) \tag{13}$$

where $\boldsymbol{V} \in \mathbb{R}^{N\times r}$ is the projection basis that approximates the aforementioned subspace and $\boldsymbol{y} \in \mathbb{R}^r$ is the respective reduced-order coordinate vector. For instance, by substituting $\boldsymbol{u}$ into the linearized form of Eq. (1), combining it with Eq. (2) and pre-multiplying with $\boldsymbol{V}^T$, thus performing a Galerkin projection, the following low-order equivalent system is derived:

$$\boldsymbol{V}^T\boldsymbol{M}\boldsymbol{V}\delta\ddot{\boldsymbol{y}}(t) + \boldsymbol{V}^T\tilde{\boldsymbol{K}}\boldsymbol{V}\delta\boldsymbol{y}(t) + \boldsymbol{V}^T\boldsymbol{G}_\star = \boldsymbol{V}^T\boldsymbol{f}(t) \tag{14}$$

which can be written as:

$$\underline{\boldsymbol{M}}\delta\ddot{\boldsymbol{y}}(t) + \underline{\tilde{\boldsymbol{K}}}\delta\boldsymbol{y}(t) + \underline{\boldsymbol{G}_\star} = \underline{\boldsymbol{f}}(t) \tag{15}$$

In both Eqs. (14) and (15), the parametric dependencies with respect to $\boldsymbol{\mu}$ have been dropped for simplification. An established approach to form the projection basis $\boldsymbol{V}$ relies on the use of POD. This technique first evaluates the FOM for a training collection of representative values of the parameters and forms the snapshot matrix:

$$\hat{\boldsymbol{S}} = \left[\, \hat{\boldsymbol{U}}(\boldsymbol{\mu}_1)\ \hat{\boldsymbol{U}}(\boldsymbol{\mu}_2) \ldots \hat{\boldsymbol{U}}\left(\boldsymbol{\mu}_{N_s}\right) \right] \tag{16}$$

where $\hat{\boldsymbol{S}} \in \mathbb{R}^{N\times(N_t\times N_s)}$ and $\hat{\boldsymbol{U}}\left(\boldsymbol{\mu}_i\right) \in \mathbb{R}^{N\times N_t}$ are the response time histories for different parameter values, henceforth termed as snapshots. Following the same notation, we can define $\hat{\boldsymbol{W}}\left(\boldsymbol{\mu}_k\right)$ as the snapshots from Eq. (10) and $\hat{\boldsymbol{Z}}\left(\boldsymbol{\mu}_k\right)$ as the snapshots from Eq. (11). Here, N_t is the number of simulation steps, $\boldsymbol{\mu}_i$ is the parametric input, and N_s is the number of snapshots. Then, the projection basis $\boldsymbol{V}$ is assembled via Singular Value Decomposition (SVD):

$$\hat{\boldsymbol{S}} = \boldsymbol{L}\boldsymbol{\Sigma}\boldsymbol{Z}^T \tag{17}$$

and truncating $\boldsymbol{L}$:

$$\boldsymbol{V} = \left[\, \boldsymbol{L}_1\ \boldsymbol{L}_2 \ldots \boldsymbol{L}_r \,\right] \tag{18}$$

where $\boldsymbol{L}_i$ are columns of matrix $\boldsymbol{L}$, henceforth termed as POD modes.

Although these definitions imply that a single projection basis is utilized, in our work, we evaluate the FOM formulation as expressed in Eqs. (10) and (11). Thus, the respective equations are projected employing POD as in Eq. (14), and a projection basis is assembled for each set of governing equations, namely $\boldsymbol{V}_w$ with respect to Eq. (10) and $\boldsymbol{V}_z$ with respect to Eq. (11). In addition, the projection-based reduction will be utilized locally for subdomains of the input parameter space. This allows the derived COR-ROM to capture parameter-dependent nonlinear behavior and localized effects accurately [63]. The assembly of the COR-ROM is described next.

4.2 Treatment due to parametric dependencies

In the case of nonlinear dynamics, the use of a single projection basis, as described in Eq. (14), which accounts for the whole parametric domain, can lead to an intractable problem or an inefficient approach [64]. Alternatively, local POD bases can be constructed for certain subdomains of the time or parameter space [47,63], capturing localized effects based on a uniform [65] or an adaptive error estimator [66,67]. In the present work, we employ the MAC as an indicator for adaptive local sampling and clustering training configurations into subsets that experience similar dynamics.

The MAC [68], also known as vector cosine or cosine similarity, is defined as a scalar constant, representing a measure of consistency between modal vectors $\boldsymbol{\phi}_r$ and $\boldsymbol{\phi}_s$ in the corresponding mathematical expression:

$$\mathrm{MAC}(\boldsymbol{\phi}_r, \boldsymbol{\phi}_s) = \frac{|\boldsymbol{\phi}_r{}^T\boldsymbol{\phi}_s|^2}{(\boldsymbol{\phi}_r{}^T\boldsymbol{\phi}_r)(\boldsymbol{\phi}_s{}^T\boldsymbol{\phi}_s)} \tag{19}$$

A MAC value that is close to 1 implies linear correspondence or a measure of the consistency of vector-based information originating from different sources. Consistent with the adopted formulation, the MAC is herein computed based on the column vectors of the $\boldsymbol{V}_z$ bases, which capture the nonlinear effects. Each projection basis captures the local underlying dynamics for each training realization through its columns $\boldsymbol{L}_i$, termed local POD modes, as expressed in Eq. (18). Therefore, the MAC can be utilized as a qualitative comparative measure of the similarity between POD modes of different parameter realizations. This provides an indirect assessment of the ability of a training realization to approximate neighboring dynamics accurately.

Thus, the MAC metric offers a twofold functionality in this work: On the one hand, it is utilized as an adaptive sampling measure that indicates if additional samples are required. It further serves as a means for subdividing the parametric input domain into clusters through the standard k-means algorithm [69]. The detailed algorithmic framework is summarized in Algorithm 1. The individual elements of the MAC-based clustering have also been validated in previous works [60,70].

Algorithm 1 The COR-ROM framework

Training Mode

1: Generate N_s random samples for the parameter vector $[\boldsymbol{\mu}_1, \boldsymbol{\mu}_2, \ldots, \boldsymbol{\mu}_{N_s}]$
2: Assume a cluster center in the closest sample to the domain's center and define d_{thr}.
3: **for** k=1,...,N_s **do**
4: Evaluate $\hat{\boldsymbol{W}}(\boldsymbol{\mu}_k)$, $\hat{\boldsymbol{Z}}(\boldsymbol{\mu}_k)$ from Eqs. 10, 11
5: Obtain $\boldsymbol{V}_{w,k}\left(\boldsymbol{\mu}_k\right)$ and $\boldsymbol{V}_{z,k}\left(\boldsymbol{\mu}_k\right)$ via POD
6: **end for**
7: Cluster samples using k-means and the MAC between bases $\boldsymbol{V}_z$ as the clustering measure d
8: Define a cluster center $\forall \boldsymbol{\mu}_k$ that $d_k \leq d_{thr}$.
9: Compute the minimum obtained MAC d_{min}.
10: **if** $(d_{min} \leq d_{thr})$ **then**
11: Refine input domain by adding $\tilde{N}_s$ samples
12: in-between $\forall(\boldsymbol{\mu}_i, \boldsymbol{\mu}_j)$ that $d_{i,j} \leq d_{thr}$
13: **go to** 3 and repeat for $k = N_{s+1}, \ldots, \tilde{N}_s$
14: **end if**

Prediction Mode

1: Deploy ROM for $\boldsymbol{\mu}_q$, with $q \notin (N_s \cup \tilde{N}_s)$
2: Identify cluster for $\boldsymbol{\mu}_q$ using nearest neighbors.
3: Evaluate ROM using $\boldsymbol{V}_w$, $\boldsymbol{V}_z$ of the cluster.

Essentially, based on the training process summarized in Algorithm 1, the framework first generates a few random samples to explore the parameter space coarsely, thus allowing for further educated refinement later on. In turn, the response of the full-order model is evaluated based on Eqs. (10) and (11), and a pair of reduced-order bases $\boldsymbol{V}_{w,k}$, $\boldsymbol{V}_{z,k}$ is computed for every parametric sample k. Then, the sampling process proceeds in a greedy fashion, utilizing the MAC values of the $\boldsymbol{V}_z$ bases as a greedy choice property to refine the number of samples in parametric domains between samples with low MAC values.

Regarding the offline computational cost, this consists of the resources needed (a) For the full-order model evaluations after each re-sampling event, (b) The respective POD reduction to obtain the projection bases, and (c) The k-means clustering technique. Since the full-order model evaluations can be performed in parallel, the computational cost of (a) equals the time needed to evaluate a single full-order model times the number of re-sampling events and typically dominates the offline portion of the method.

Finally, as explained, the initial sampling during the first step of the algorithm is performed randomly. As the number of parameters N_p increases, more refined approaches might be required to mitigate potential bottlenecks due to the curse of dimensionality. This discussion extends beyond the scope of this paper, however, the interested reader can refer to [71–73].

4.3 Hyper-reduction

The final component of the proposed framework is a second-tier approximation technique, termed hyper-reduction, which critically influences efficiency as it allows for updating and reconstructing the restoring force term in an online manner, despite its nonlinear nature [74]. This strategy allows evaluating the projections of the nonlinear terms only at a subset of the total number of discrete elements, thus yielding a substantial reduction of the involved computational toll.

As the parametric dependencies used in this problem are not necessarily affine, and the investigated problems are of a nonlinear nature, we adopt an Energy Conserving Mesh Sampling and Weighting (ECSW) [75,76], which has been tested for such applications. Based on the original formulation, the ROM matrices are approximated as follows:

$$\tilde{\boldsymbol{K}} = \sum_{e=1}^{n_e} \boldsymbol{V}_e^T \tilde{\boldsymbol{K}}_e \boldsymbol{V}_e \approx \sum_{e \in \tilde{E}} \xi_e \boldsymbol{V}_e^T \tilde{\boldsymbol{K}}_e \boldsymbol{V}_e$$
$$\boldsymbol{G} = \sum_{e=1}^{n_e} \boldsymbol{V}_e^T \boldsymbol{G}_e \approx \sum_{e \in \tilde{E}} \xi_e \boldsymbol{V}_e^T \boldsymbol{G}_e \tag{20}$$

where the total number of elements is denoted by n_e, $\boldsymbol{V}_e$ contains a subset of rows of $\boldsymbol{V}$ corresponding to the DOFs of element e and $\tilde{E}$ represents a subset of the elements, such that $\left|\tilde{E}\right| \ll n_e$, whereas $\tilde{\boldsymbol{K}}_e$ and $\boldsymbol{G}_e$ are the system matrices of element e, as described in Eq. (4). Similar approximations hold for the mass and damping matrices $\boldsymbol{M}, \boldsymbol{C}$. The coefficient term ξ_e is a weight contribution of element e in the system matrices.

To determine the element subset $\tilde{E}$ and weights ξ_e we rely on an energy-based approach, as documented in detail in [55]. In short, subset $\tilde{E}$ and weights ξ_e are computed so that the overall work produced over this subset, weighed by the respective coefficients, sufficiently approximates the work produced over the full mesh for a set of training configurations. Therefore, the following column matrix is assembled:

$$\boldsymbol{P}_e^{i,j} = \boldsymbol{V}_e^T \boldsymbol{G}_e \left(\boldsymbol{\mu}_i, \boldsymbol{u}_e^j\right), \quad \boldsymbol{b}^{i,j} = \sum_{e=1}^{n_e} \boldsymbol{P}_e^{i,j} \tag{21}$$

where $\boldsymbol{P}_e^{i,j}$ is the entry of the matrix that corresponds to the work produced in element e over each column of $\boldsymbol{V}_e$ at time step j for the parameter vector $\boldsymbol{\mu}_i$, whereas the vector $\boldsymbol{b}^{i,j}$ follows the same notation regarding the total work produced over the whole mesh. By computing these terms for several parametric configurations and simulation steps or non-converged return mapping iterations, the following is derived:

$$\boldsymbol{P} = \begin{bmatrix} \boldsymbol{P}_1^{1,1} & \dots & \boldsymbol{P}_{n_e}^{1,1} \\ \vdots & \ddots & \vdots \\ \boldsymbol{P}_1^{1,2} & \dots & \boldsymbol{P}_{n_e}^{1,2} \\ \vdots & \ddots & \vdots \\ \boldsymbol{P}_1^{N_s,\bar{n}_t} & \dots & \boldsymbol{P}_{n_e}^{N_s,\bar{N}_t} \end{bmatrix} \quad \boldsymbol{b} = \begin{bmatrix} b^{1,1} \\ \vdots \\ b^{1,2} \\ \vdots \\ b^{N_s,\bar{N}_t} \end{bmatrix} \tag{22}$$

where N_s is the number of training samples and $\bar{N}_t$ is the number of iterations considered. With these computations in place, subset $\tilde{E}$ and weights ξ_e can be obtained based on the following optimization problem:

$$\boldsymbol{\xi}^* = \arg\min_{\boldsymbol{\xi}\in\Phi} \|\boldsymbol{\xi}\|_0 \tag{23}$$

with,

$$\Phi = \boldsymbol{\xi} \in \mathbb{R}^{n_e} : \|\boldsymbol{P}\boldsymbol{\xi} - \boldsymbol{b}\|_2 \leq \tau \|\boldsymbol{b}\|_2 , \ \xi_e \geq 0 \tag{24}$$

where $\|\bullet\|_0$ and $\|\bullet\|_2$ represent the L_0 and L_2 norm, respectively. Term τ denotes a user-defined tolerance that controls the quality of the approximation, whereas Φ represents a set of candidate solutions. Upon solution, subset $\tilde{E}$ is obtained directly from the non-zero elements of $\boldsymbol{\xi}^*$. The former minimization problem is typically solved via the sparse Non-Negative Least Squares (sparse NNLS) algorithm [77].

5 Numerical examples

In this section, the performance of the proposed ROM framework is tested. A four-story, three-dimensional frame featuring hysteretic nonlinearities at the location of the joints (localized regions) is investigated first as a toy example, which serves for illustration and discussion on performance. A large-scale kingpin system is examined as the next example, where the weld region is assumed to represent an individual component characterized by plasticity [78].

5.1 Error measures and timings

The proposed framework is entirely implemented in an in-house developed FE code in MATLAB and tested in a workstation equipped with an Intel Xeon E3-1585 quad-core processor, running at 3.70GHz, and 32GB of memory. For a fair comparison, numerical integration is performed by means of an implicit Newmark scheme, which uses the same integration discretization and time step for both the ROM and FOM. Moreover, the speed-up factor, which serves as a measure of efficiency, is calculated as the ratio of CPU time required for the ROM evaluation over the time needed for the FOM simulation. The reported timings are averaged over the respective training or testing configurations set. The accuracy of the ROM framework is quantified on the basis of the normalized L_2 norm of the difference of the nonlinear quantity of interest Q at selected DOFs and time steps, relying on the following equations:

$$\begin{aligned} \text{Error} &= \sum_{i\in\tilde{N}_{\text{dof}}} \sum_{j\in\tilde{N}_t} \left(Q^j_{\text{FOM},i} - \tilde{Q}^j_{\text{ROM},i} \right)^2 \\ \text{Ref} &= \sum_{i\in\tilde{N}_{\text{dof}}} \sum_{j\in\tilde{N}_t} \left(Q^j_{\text{FOM},i} \right)^2 \\ Q_{\text{error}} &= \frac{\sqrt{\text{Error}}}{\sqrt{\text{Ref}}} \times 100\% \end{aligned} \tag{25}$$

Performance is examined with respect to the recovery of ground truth displacements in the isolated nonlinear region and stresses.

To gain a deeper insight into the potential and limitations of the proposed framework, four different ROM configurations are examined. First, a global ROM termed GROM is assembled, which utilizes a single global basis for the whole system and all inputs extracted from the training snapshots of the entire domain. No clustering is required in this case. The second ROM, termed Iso-ROM, relies on the substructural formulation explained in Sect. 3 but only reduces the linear components of the structure.

Thus, it only assembles the local $\boldsymbol{V}_w$ and projects the governing set of equations for the linear components (Eq. 10), whereas the response in the welding region is evaluated in the full coordinate space. In this case, clustering is employed, as described in Sect. 4.2. The last two parametric ROMs are derived based on the framework described in Sect. 4, utilizing both $\boldsymbol{V}_w$

Table 1 Reference notation table for ROMs variations utilized for comparison and validation purposes

Name	Description
FOM	The full-order model of the system
GROM	A global basis based on training snapshots of the entire domain
Iso-ROM	Reduction on monolithic response in Eq. (10), assemble of V_w, isolated region(s) in full coordinates (Eq. (11)). A V_w basis per cluster.
COR-ROM	Component-Oriented Reduction-ROM, as presented in Sect. 4. A V_w and a V_z basis per cluster, component-oriented treatment.
HpGROM	The GROM additionally equipped with hyper-reduction
HpCOR-ROM	COR-ROM additionally equipped with hyper-reduction

and $\boldsymbol{V}_z$ for the individual reduction of each component. The performance is evaluated with and without the hyper-reduction approximation of Sect. 4.3. The configurations of these four different ROMs are summarized in Table 1, along with their reference names used throughout this study.

5.2 Four-story shear frame with multiple localized nonlinearities

We consider a FE model of a three-dimensional four-story frame with hysteretic links subjected to ground motion as an initial proof of concept example. The nonlinear behavior of each link is described by a Bouc-Wen hysteretic model [79,80]. This multi-DOFs simulator is chosen as a demonstrative example due to its modularity in terms of defining a multi-DOF nonlinear system when adding stories and frames. This setup is characterized by localized regions of nonlinearity (at the joints), which reproduce complex nonlinear effects (hysteresis and degradation), thus challenging the performance limits of our ROMs. In addition, this example has already been utilized in similar model-order reduction studies [46,81,82], thus enabling results comparison and reproduction. The configuration of the frame relies on a published benchmark case study of a multi-degree of freedom nonlinear response simulator [61,62], where virtual nodes are introduced in each coupling to materialize nonlinear joint behavior. The model setup is described first in short. The ground motion parameterization is presented next before reporting the performance of the derived COR-ROM.

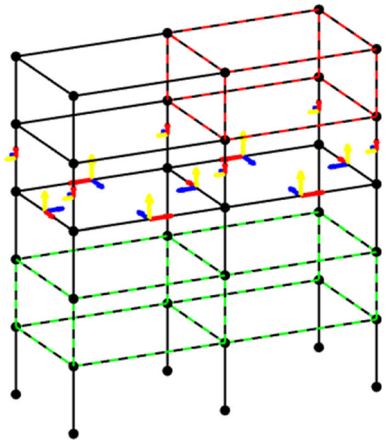

Fig. 3 Configuration of the four-story shear frame. The dashed-colored beams indicate the nonlinear regions

5.2.1 Model setup

A graphical illustration of the setup is presented in Fig. 3. The hysteretic links assume no length, and the respective virtual nodes are defined as duplicates of the existing discretization. For more details on the assembly and the respective assumptions, the interested reader is referred to [61].

The case study follows the template configuration in terms of material properties definitions. Specifically, steel HEA cross-sections have been used for all beam elements, whereas the structure is assembled using two horizontal frames, each of 7.5 ms in length and one frame of six meters along the width. In addition, the modularity of the simulator is exploited to assemble four stories along the height, each one of 3.2 ms, and define two distinct nonlinear isolated regions to validate the proposed COR-ROM of Table 1. Rayleigh proportional damping is also assumed, corresponding to 2% modal damping, ascribed to the structure's first and second global modes. The setup is illustrated in Fig. 3, where the shear frame is modified compared to the original benchmark in [61], and the hysteretic couplings are activated only on the colored regions.

Therefore, based on the benchmark description, the restoring force of each link in the shear frame simulator

of Fig. 3 can be decomposed in a linear and a hysteretic term. The respective mathematical formulation reads:

$$\begin{aligned}\mathbf{R} &= \mathbf{R}_{\text{linear}} + \mathbf{R}_{\text{hysteretic}} \\ &= \alpha k \mathbf{du} + (1-\alpha) k \mathbf{z}\end{aligned} \tag{26}$$

where $\mathbf{R}$ denotes the vector of restoring forces, $\mathbf{du}$ represents the nodal displacements, and α, k are traits characterizing the Bouc-Wen model on each link. Variable $\mathbf{z}$ controls the hysteretic term of the restoring force and obeys the following:

$$\dot{\mathbf{z}} = \frac{A\mathbf{d}\dot{\mathbf{u}} - \nu(t)(\beta|\mathbf{d}\dot{\mathbf{u}}|\mathbf{z}|\mathbf{z}|^{w-1} - \gamma\mathbf{d}\dot{\mathbf{u}}|\mathbf{z}|^{w})}{\eta(t)} \tag{27}$$

where,

$$\begin{aligned}&\nu(t) = 1.0 + \delta_\nu \epsilon(t), \quad \eta(t) = 1.0 + \delta_\eta \epsilon(t), \\ &\epsilon(t) = \int_0^t \mathbf{z}\mathbf{d}\dot{\mathbf{u}}\mathrm{d}t\end{aligned} \tag{28}$$

Parameters A, β, γ, and w in Eq. (27) define the shape and amplitude of the hysteretic curve that characterizes the dynamic behavior of each link. Additional strength deterioration or stiffness degradation effects can be modeled via $\nu(t)$ and $\eta(t)$ in Eq. (28), respectively, whereas $\epsilon(t)$ stands for the absorbed hysteretic energy.

This parameterized shear frame simulator is utilized to verify the derived ROMs in terms of reproducing the (rapidly) varying nonlinear behavior of the frame based on the parametric input of the system described in Sect. 5.2.2. To additionally model localized nonlinear regions that can be treated as individual components and validate the substructural formulation of the proposed COR-ROM, only the links pertaining to the colored regions of Fig. 3 are activated. The remaining couplings are assumed to be described by a linear regime, which is enforced by setting $\alpha = 1$ in Eq. (26).

5.2.2 Excitation's parameterization

The earlier described numerical system setup allows us to account for parametric dependencies pertaining to the structural properties, as defined in terms of the characteristic traits of the nonlinear links. However, our goal is to address generalized case studies, where dependencies on both the defining system parameters as well as the characteristics of the forcing input are tackled. Thus, we here further consider a parameterization of the ground motion, similar to the process demonstrated in previous work of the authoring team [82,83].

Specifically, the stochastic model for (synthetic) ground motion signals proposed in [84] produces realistic yet synthetic acceleration signals by filtering, normalizing, and time-modulating a white noise signal. An overview of the respective process is visualized in Fig. 4. The time-modulating filter relies on the following non-stationary function:

$$\mathbf{q}\left(t, d_1, d_2, d_3\right) = d_1 t^{d_2 - 1} exp\left(-d_3 t\right) \tag{29}$$

where $\mathbf{d} = [d_1, d_2, d_3]$ define the intensity, the shape, and the duration of the motion, respectively. A direct link exists between these parameters and the temporal characteristics of the excitation: (a) The expected Arias intensity I_A, (b) The effective duration of the motion D_{5-95} and (c) The time-mark t_{mid} at which a 45% level of I_A has been reached. In addition, the time-varying filter in Fig. 4 is implemented via an Impulse Response Filter as follows:

$$h\left[t - \tau\right] = \frac{\omega_f\left(\tau\right)}{\sqrt{1-\zeta^2}} \exp\Omega_1 \sin\Omega_2 \tag{30}$$

where,

$$\begin{aligned}\Omega_1 &= \left[-\zeta\omega_f\left(\tau\right)\left(t-\tau\right)\right] \\ \Omega_2 &= \left[\omega_f\left(\tau\right)\sqrt{1-\zeta^2}\left(t-\tau\right)\right]\end{aligned} \tag{31}$$

Here, the damping ratio is denoted by ζ_f, ω_f is the filter's frequency with $\omega_f = \omega_{\text{mid}} + \omega'\left(\tau - t_{\text{mid}}\right)$, whereas ω' represents the rate of change of ω, and ω_{mid} is the frequency at $t = t_{\text{mid}}$. An algorithmic implementation is published in [85]. With this stochastic process in place, the temporal and spectral characteristics of the ground motion accelerograms can be treated as input parameters in the aforementioned COR-ROM, thus allowing for a parametric representation of a target signal or a set of them. Thereafter, the ROM can be validated using "synthetic" ground motion signals, equivalent to the target (or real recorded) ones with respect to the similarity of their time-frequency characteristics [83].

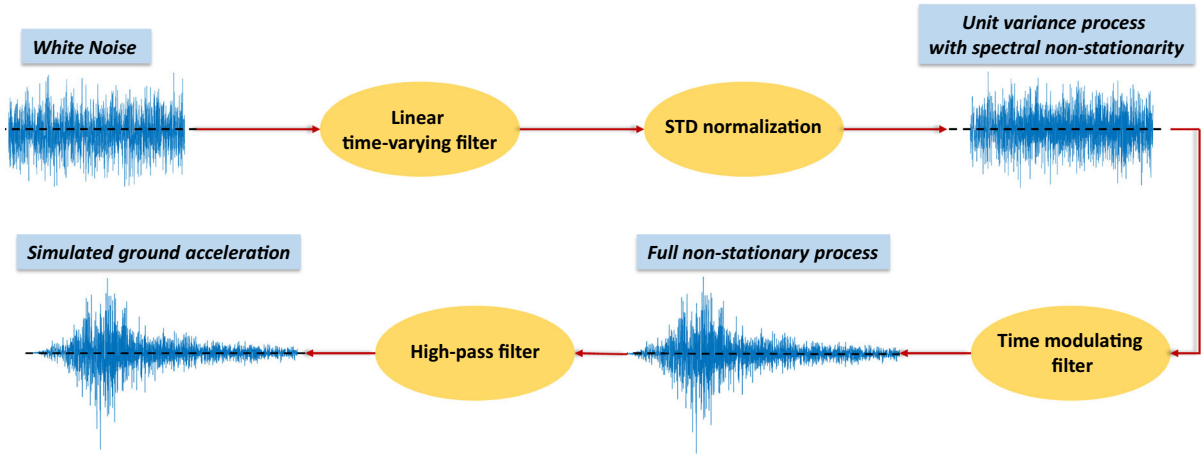

Fig. 4 Process workflow to produce synthetic accelerograms based on [84]

5.2.3 Model parametric dependencies

With the model setup and the stochastic framework for parameterization of the ground motion excitation in place, the assumptions regarding the dependencies of the high-fidelity FE model, which represents the FOM, can now be defined.

As already explained, the proposed approach targets systems comprising multiple components and attempts to derive a surrogate able to capture the system's response over a domain of parameters that define its input loading or initial state, thus dictating its dynamic behavior. In this work, both global system parameters and parametric traits of the excitation are injected into the proposed COR-ROM, along with characteristics that define the behavior of local components. Using such a modular parameterized case study allows us to illustrate the generalization potential of the proposed formulation. In Table 2, the respective modeling assumptions are summarized.

Regarding the system properties, two traits of the nonlinear joints of the shear frame in Fig. 3 are treated in a parametric manner to simulate a variety of qualities and shapes of the corresponding hysteresis curves. Specifically, parameters α and k in Eq. (26) are modeled as dependencies in the isolated regions of Fig. 3, whereas in the rest of the frame, the nonlinear links are not activated by setting $\alpha = 1.0$ in Eq. (26). Parameter α functions as a weighting factor between the hysteretic and linear term of the restoring force, whereas parameter k introduces weakened components as it corresponds to the link's stiffness. These assumptions imply

Table 2 Modeling assumptions for the shear frame inputs

Global structure
$E = 210$ GPa, $k = 2.5e^8$, $\alpha = 1.0$
1st story isolated region
$[\beta, \gamma, w, A] = [3.0, 2.0, 0.5, 1.0]$
$k_1 \sim \mathcal{N}(1.35e^8,\ (8e^6)^2)$, $\alpha_1 \sim U[0.2, 0.4]$
4th story isolated region
$[\beta, \gamma, w, A] = [2.0, 3.0, 0.5, 1.0]$
$k_4 \sim \mathcal{N}(1.20e^8,\ (8e^6)^2)$, $\alpha_4 \sim U[0.35, 0.60]$
Excitation parameters
$[\omega', \zeta, t_{\text{mid}}, D_{5-95}] = [-0.416, 0.251, 0.129, 0.408]$
$\omega_{\text{mid}}(Hz) \sim \mathcal{LL}(3.52, 0.24)$, $\sqrt{(I_A)} \sim \mathcal{IG}(0.26, 0.11)$

Parameters $\alpha, k, \beta, \gamma, w, A$ refer to the hysteretic links and the rest to the synthetic excitation

a parameter-dependent matrix $\tilde{\boldsymbol{K}}(\boldsymbol{\mu}, \delta\boldsymbol{u})$ for the system, as presented in Eq. (2), as every parametric realization $\boldsymbol{\mu}$ leads to a model evaluation with different stiffness for the nodal couplings.

Regarding the input excitation $\boldsymbol{f}(\boldsymbol{\mu}, t)$ in Eq. (2), a ground motion scenario is adopted. Specifically, the structure is excited using a ground motion signal, whose direction is defined in the $(x - y)$ plane representing the ground. Specifically, the direction of the motion is modeled through its angle $\phi = \pi/4$ with respect to the longitudinal axis of the frame. In addition, the temporal and spectral characteristics of the input signal are also treated as parametric dependencies using the already introduced stochastic modeling

framework. The respective probability density functions (pdf) for each input parameter are summarized in Table 2, and are selected based on the suggestions in [83], where the pdf of each parameter has been fitted on actual ground motion samples extracted from the PEER Ground Motion Database [86]. The parameters that are not modeled using a pdf are considered constant and equal to the most probable value according to the distributions specified in [83].

5.2.4 Performance evaluation

The numerical experiment is designed, on the basis of the parametric inputs of Table 2, adopting a Latin Hypercube Sampling (LHS) strategy utilizing 250 training samples and 1000 validation configurations. Relying on previous works validating ROM performance on this same benchmark example, a reduction order of $r_w = 4$ is chosen for $\boldsymbol{V}_w \in \mathbb{R}^{996\times 4}$, whereas $r_z = 16$ is selected for each localized basis so that $\boldsymbol{V}_z \in \mathbb{R}^{312\times 16}$ and $\boldsymbol{V}_z \in \mathbb{R}^{192\times 16}$ for the first and top story, respectively. A total number of 22 clusters were used for the COR-ROM. For the global $GROM$ in Table 2 the reduction order is set to $r = 32$. Due to the number of DOFs of the benchmark, the hyper-reduced variation of the COR-ROM is not evaluated here, as the system is too small to demonstrate any substantial computational savings.

The ability of the proposed COR-ROM to approximate the underlying nonlinear effects on the isolated components of the system is summarized in Table 3. The physics-based nature of the reduction leads to a low-order equation of motion as expressed in Eq. (15), enabling the derived surrogate, termed COR-ROM, to integrate the dynamics forward in time for varying conditions and dependencies efficiently, yielding full-field estimates of the dynamic response, including displacements, accelerations, energy measures and even stresses or strains. For instance, accelerations is one of the primary fields being monitored in SHM case studies. Thus, the ability of the derived ROM to infer the underlying dynamics as expressed in terms of accelerations is crucial for the utility and serviceability of the ROM as part of a SHM framework. Strain and stresses can be inferred simultaneously but are omitted here for the sake of demonstration.

The performance between the ROMs reported in Table 1 is also compared in Table 3. As expected, the GROM that utilizes a single global projection basis for the whole system and the entire domain of inputs cannot accurately reproduce the system's time response. The respective error measures indicate that the GROM fails to capture both the localized effects of the shear frame in the isolated regions, as reflected in $\boldsymbol{Z}$, and the global response of the system. This further documents the necessity for a component-oriented treatment of such an assembly system. In this context, the derived Iso-ROM that evaluates the deviatoric response $\boldsymbol{Z}$ in Eq. (11) in full coordinates and reduces only Eq. (10) outperforms all other representations and delivers high-precision estimates. This implies that the nonlinear features of the isolated regions play a dominant role when trying to capture the dynamic response and might make the ROM's performance deteriorate if not reproduced sufficiently. Thus, a component-oriented treatment is deemed necessary.

However, the Iso-ROM may eventually suffer from efficiency limitations since the response evaluation of the nonlinear component in full-order leads to considerable computational toll and cannot guarantee (near) real-time model evaluations. Even though the small size of this proof-of-concept example is not suitable to properly demonstrate this effect, the average speed-up the Iso-ROM achieves compared to the FOM evaluations is 1.52 and is still lower than the one by GROM or COR-ROM equal to 2.36 and 2.21, respectively. For the sake of completeness, the offline cost of the method is 912 s, and the average time required for a full-order model evaluation is 189 s. Thus, reduction in the isolated regions is not an option but a necessity for low-order representations that are to be exploited in the context of twinning or real-time diagnostics SHM frameworks, where accelerated or real-time estimations are necessary.

Although the proposed COR-ROM yields higher approximation errors and a few more performance outliers as compared against the Iso-ROM in Fig. 5, its overall performance in terms of capturing the time history response of the system is sufficiently accurate and a necessary trade-off that guarantees efficiency. In any case, the proposed COR-ROM delivers a superior approximation in terms of quality compared to GROM, and its robustness is also highlighted in Fig. 5, where the number of outliers is negligible compared to the size of the validation set.

To further demonstrate the precision of the proposed framework and argue why the approximations of the COR-ROM are deemed sufficiently accurate in the con-

Table 3 Performance for the ROMs from Table 1 for the shear frame. The average and maximum measures of Eq. (25) are presented for the response in the isolated region, along with the error in two examples

	Average error		Maximum error	
	Z_{error} (%)	$\ddot{Z}_{\text{error}}$ (%)	Zerror (%)	$\ddot{Z}_{\text{error}}$ (%)
GROM	21.5	36.6	27.3	38.1
Iso-ROM	1.8	7.4	6.5	15.3
COR-ROM	4.4	10.5	12.0	15.8
	Sample A[a]		Sample B[b]	
	Z_{error} (%)	$\ddot{Z}_{\text{error}}$ (%)	Z_{error} (%)	$\ddot{Z}_{\text{error}}$ (%)
GROM	22.0	34.4	21.5	35.8
Iso-ROM	1.7	6.1	1.8	5.6
COR-ROM	5.5	11.4	6.7	13.3

[a] $k_1 = 1.35e^8$, $\alpha_1 = 0.31$, $k_4 = 1.12e^8$, $\alpha_4 = 0.51$, $\omega_{\text{mid}} = 24$, $\sqrt{I_A} = 0.16$.
[b] $k_1 = 1.43e^8$, $\alpha_1 = 0.23$, $k_4 = 1.20e^8$, $\alpha_4 = 0.37$, $\omega_{\text{mid}} = 32$, $\sqrt{I_A} = 0.30$

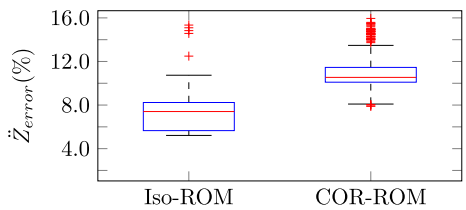

Fig. 5 Precision boxplots with respect to the acceleration response in the nonlinear regions

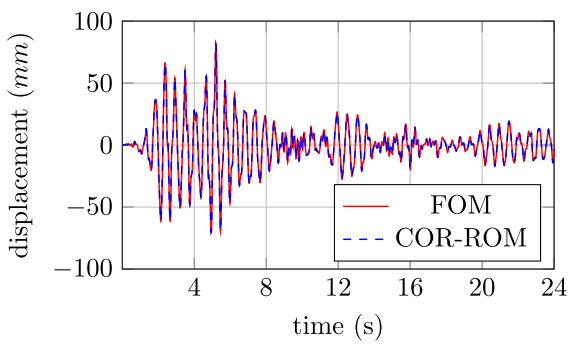

Fig. 6 Response approximation for the shear frame at the maximum displacement DOF for Sample A

text of SHM applications, the time history estimation of the top story behavior of the frame is illustrated in Fig. 6 for Sample A and in Fig. 7 for ample B, as reported in Table 3. The accuracy for these two samples is close to the average measure reported in Table 3, so they are adopted as characteristic instances for illustrating the COR-ROM's performance.

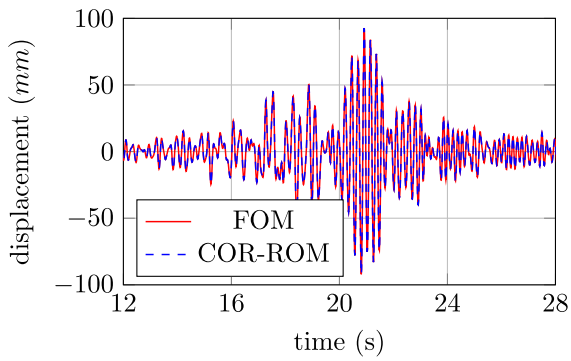

Fig. 7 Response approximation for the shear frame at the maximum displacement DOF for Sample B

The respective hysteretic curves of the top right horizontal nodal coupling are also depicted in Fig. 8 to demonstrate an example of the variety of different nonlinear phenomena that dominate the behavior of the frame. The derived COR-ROM captures the underlying system behavior in a robust manner, as implied by the respective approximation for these two earthquake-like ground motions that induce significant nonlinearity, as evidenced by the resulting hysteretic curves.

The COR-ROM is next verified on a large-scale example featuring material plasticity, where computational efficiency and hyper-reduction are also considered to explore the possibility of (near) real-time model evaluations of complex systems.

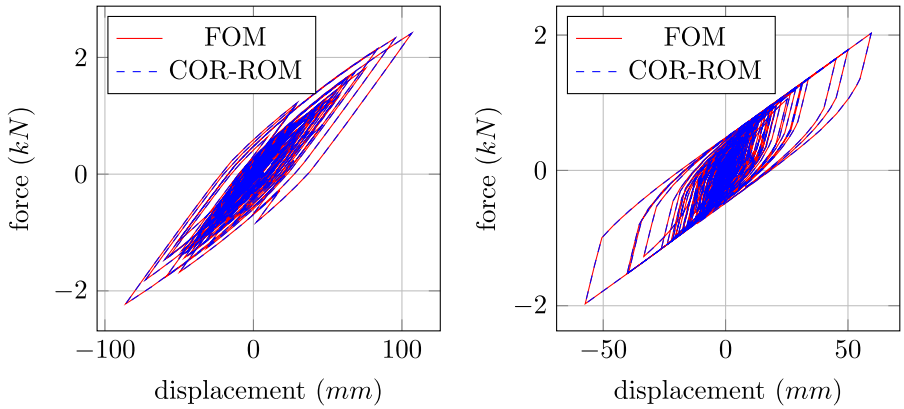

Fig. 8 COR-ROM approximation of the hysteresis curve of the shear frame at the maximum displacement DOF for Sample A (left) and Sample B (right)

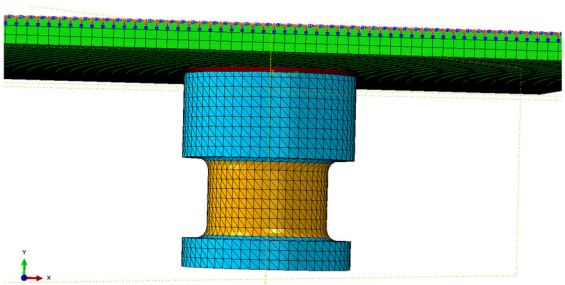

Fig. 9 FE model for the kingpin connection. The nonlinear welding region and excitation domain are depicted in red and orange, respectively

Table 4 Geometrical and material properties for the components of the kingpin system

Upper plate
Young modulus E = 200 GPa, Density $\rho = 8100\,\mathrm{kg/m^3}$
Poisson Ratio $\nu = 0.30$, Thick. = 10 mm, Edge = 300 mm
Welding region
Young modulus E = 198 GPa, Density $\rho = 7850\,\mathrm{kg/m^3}$
Poisson Ratio $\nu = 0.30$, Thick. = 2 mm, Radius = 74 mm
Kingpin
Young modulus E = 210 GPa, Density $\rho = 7850\,\mathrm{kg/m^3}$
Poisson Ratio $\nu = 0.32$, Height = 83 mm

5.3 Large-scale kingpin connection

The performance of the proposed COR-ROM and the comparative alternatives, summarized in Table 1, are cross-assessed here for the case of a large-scale kingpin connection system, where the weld region is characterized by plasticity. Both accuracy and efficiency considerations are considered for this example. Plasticity is only modeled for the welding component of the system, assuming it represents a weak spot in the system. The model setup is presented next, followed by the ROM framework details and the numerical results.

5.3.1 Model setup

The model setup is summarized in Table 4, and its discretization is illustrated in Fig. 9. In terms of implementation, the green component representing the upper steel plate of the system is discretized using 12150 elements, whereas its top surface is considered fully bounded, as depicted in Fig. 9. In addition, the welding region consists of 11543 elements and is depicted in red, whereas the kingpin component is illustrated in cyan and has 28351 elements.

Linear elastic material properties are assumed for the plate and the kingpin, while the circular welding region materializing their connection follows a von Mises plasticity rule. The respective geometric and material properties are summarized in Table 4. Rayleigh proportional damping is assumed, corresponding to 2% modal damping ascribed to the structure's first and second global modes. The system is excited using nodal forces applied at the orange region depicted in Fig. 9. Specifically, this region represents the domain where a vehicle's trailer (truck) is connected to the tractor; this drives the truck forward through the kingpin and the corresponding fifth-wheel connection. The applied forcing in this domain represents the traction and pulling forces or vibrations coming from the trailer during driving or steering. A parameterized dynamic acceleration signal is considered as an input, applied

Table 5 Parametric dependencies of the FOM model of the kingpin connection

Excitation amplitude	$Amp \sim \mathcal{N}\left(100, 6^2\right)$
Excitation direction	$\theta \sim \mathcal{U}\left(\frac{\pi}{6}, \frac{\pi}{3}\right)$
Yield stress of welding region	$f_y \sim \mathcal{N}\left(435, 7^2\right)$ MPa

to the discretization nodes of the highlighted orange region in Fig. 9.

5.3.2 Dependencies and ROM setup

Similar to the shear frame case study, the derived ROM is validated with respect to its ability to reproduce the dynamic response under various acting parametric inputs. In this case, uncertainty is injected into the framework in the system properties and the characteristics of the excitation. Specifically, the imposed acceleration signal, which is applied at the orange region illustrated in Fig. 9, is modeled as a stochastic multi-sinusoidal signal. Its amplitude Amp is assumed to follow a normal distribution, whereas its (x-z) in-plane direction of motion is modeled through angle θ that follows a uniform distribution. In turn, when multiplying this acceleration signal with the mass matrix, it leads to the parametric-dependent excitation $\boldsymbol{f}(\boldsymbol{\mu}, t)$ in Eq. (1). In addition, the yield stress of the welding region further follows a normal distribution. This implies a parameter-dependent matrix $\tilde{\boldsymbol{K}}(\boldsymbol{\mu}, \delta\boldsymbol{u})$ as presented in Eq. (2), since the reconstruction of the tangent stiffness matrix during every simulation step relies on the nonlinear constitutive law. The respective assumptions are summarized in Table 5.

Following a strategy similar to the shear frame case study, the training is designed using a LHS design to sample the input parametric domain to obtain the required training simulations. As explained in Sect. 4.2, an adaptive sampling strategy is employed along with clustering to search the parameter space and construct accurate local bases efficiently. The number of clusters is manually set to 10, whereas the size of the two bases is selected so that the resulting displacement response error on the global system and the localized nonlinear region does not exceed a certain threshold, in the present case 1%. In this manner, each validation parametric sample is assigned to a cluster through the standard k-means algorithm. The cluster's projection bases are used to perform the reduction based on Sect. 4.

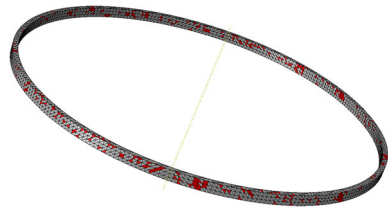

Fig. 10 ECSW mesh for the kingpin connection highlighted in red for one of the clusters

The same applies to the hyper-reduction approximation, as each cluster retains its own subset of elements $\tilde{E}$ and weight coefficients $\boldsymbol{\xi}_e$ in Eq. (20). As nonlinearity is only featured in the welded region, the hyper-reduction approximation is applied only to the weld elements. An example visualization is provided in Fig. 10. Thus, the framework ends up using 56 training snapshots and a reduced dimension of $r_w = 4$ for $\boldsymbol{V}_w$ regarding the projection of the linear components (Eq. 10) and $r_z = 16$ for $\boldsymbol{V}_z$ with respect to Eq. (12) and the nonlinear welding region. For the sake of completeness, the offline cost of the method is 41152 s, and the average time required for a full-order model evaluation is 13221 s.

5.3.3 Performance evaluation

The framework's performance is validated on a set of 250 parametric realizations not included in the training set. The respective accuracy in capturing the behavior of the FOM in terms of displacements and stresses is evaluated. The error measure of Eq. (25) is computed for each component separately, whereas the respective stress approximation is computed after post-processing for the subset of elements $\tilde{E}$ retained by the hyper-reduction approximation. The subset $\tilde{E}$ is visualized in Fig. 10 for one of the clusters used.

The ability of the proposed COR-ROM to capture the underlying full-order dynamic behavior is presented in Figs. 11 and 12.

First, the accuracy of the COR-ROM of Table 1 is presented to validate the proposed framework, compared against the respective FOM response. Based on the overall evaluation of the ROM, the validation sample is selected for demonstration so that the framework delivers its average performance. The respective approximation is evaluated for each component separately. Thus, Fig. 11 presents the ROM performance in the linear region of the model, whereas Fig. 12 evaluates the approximation in the welding region where

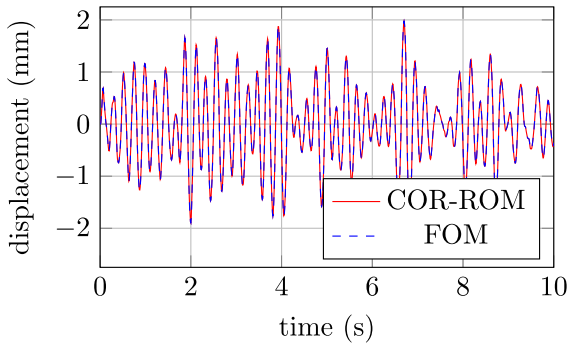

Fig. 11 Time history approximation in the kingpin at the maximum displacement DOF for $Amp = 132$, $\theta = \pi/4$, and $f_y = 421$ MPa

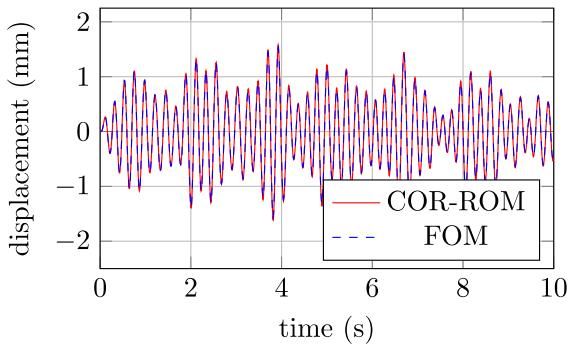

Fig. 12 Time history approximation in the welding region at the maximum displacement DOF for $Amp = 132, \theta = \pi/4$, and $f_y = 421$ MPa

nonlinearity in the form of plasticity is present. The framework delivers a more accurate performance for the linear region, as illustrated in Fig. 11, where the respective time histories are practically indistinguishable. In addition, it captures the dynamics of the isolated nonlinear region in Fig. 12.

Although discrepancies in the performance in each component are evident, the framework manages to reproduce the overall underlying response with sufficient accuracy, indicating its suitability for condition monitoring or similar SHM-related tasks. As a reminder, the hyper-reduced version HpCOR-ROM utilizes an additional second-tier approximation for the nonlinear terms on the isolated region to achieve efficiency, and the respective accuracy is expected to deteriorate. Thus, the derived COR-ROM prior to hyper-reduction needs to deliver a high-precision approximation as it does in Fig. 12.

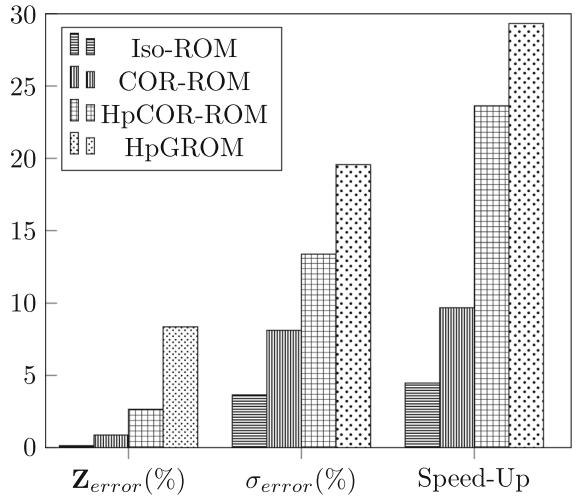

Fig. 13 Average performance comparison for the ROMs of Table 1 for the kingpin connection

A quantification of the performance of the reduction schemes that are summarized in Table 1 is illustrated in Fig. 13 for comparison purposes. The average accuracy for the displacement time history $\boldsymbol{Z}$ in the nonlinear welding region and the stresses σ in the nonlinear component are shown, along with the respective speed-up factor for each of the implemented ROMs. This illustration serves as a comparison that demonstrates the respective advantages of utilizing the proposed COR-ROM, or its hyper-reduced variant HpCOR-ROM, instead of adopting a global reduction strategy or the full-order evaluation of the nonlinear component, termed as Iso-ROM.

As already explained, the HpGROM yields the highest error, thus proving to be unreliable for SHM tasks, although the achieved speed-up is considerable due to hyper-reduction. This implies that the assembled global basis cannot accurately capture the localized nonlinear phenomena. Even if we increase the size of the global basis and truncate using more modes in Eq. (17), efficiency will be compromised even more, thus not allowing for online model evaluations. Since the nonlinear features are present only in a local component, the global modes of the respective basis cannot capture the dynamics sufficiently, indicating that an alternative approach that adopts some form of localized treatment is needed.

In contrast, the derived Iso-ROM of Table 1 that reduces only the linear components of the system and evaluates the isolated region in full coordinates

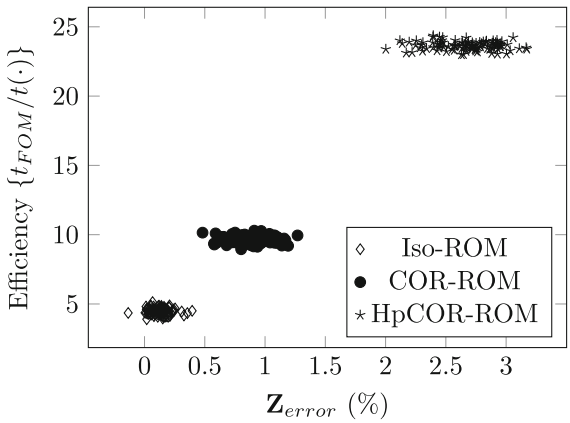

Fig. 14 Efficiency to accuracy relation for the ROMs of Table 1 for the kingpin connection

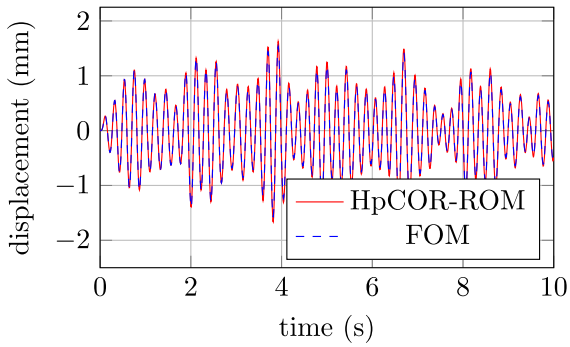

Fig. 15 Time history HpCOR-ROM approximation in the welding region at the maximum displacement DOF ($Amp = 132$, $\theta = \pi/4$, $f_y = 421$ MPa)

achieves a high-precision estimation. The average accuracy in Fig. 13 is improved substantially, as, in this case, the nonlinear terms are evaluated in an exact manner. In addition, the Iso-ROM demonstrates the most robust performance, as illustrated in Fig. 14 where the efficiency to accuracy relation is depicted for every validation sample. However, the Iso-ROM 's major disadvantage is its limited ability to provide accelerated computations, as it evaluates the nonlinear terms in FOM coordinates. Specifically, in this example where the nonlinear region is relatively large, the Iso-ROM delivers a rather insignificant speed-up.

On the other hand, the proposed COR-ROM provides a sufficiently accurate approximation for SHM purposes, and, when equipped with hyper-reduction to form HpCOR-ROM, achieves a significant speed-up that can potentially enable near real-time evaluations. This is demonstrated in Fig. 14, where the HpCOR-ROM accelerates the model evaluations by a factor of 24 while retaining an accurate approximation with less than 3.5% error on capturing the response in the nonlinear welding region. The quality of the HpCOR-ROM estimation is also depicted in Fig. 15 for the welding region. The same degree of freedom and parametric input as in Fig. 12 has been chosen to demonstrate the discrepancy introduced due to the hyper-reduction component of the COR-ROM. The respective trade-off that the HpCOR-ROM introduces seems acceptable, as, despite the minor deterioration of the ROM's accuracy, the yielded speed-up is substantial and key to effectuating of real-time downstream tasks (e.g., those related to SHM). These performance measures are further summarized in Table 6.

6 Conclusions

We introduce a reduced-order modeling framework, relying on adoption of a substructuring formulation that allows individual component treatment. Specifically, a decomposition of the response is introduced by using a coordinate separation, which succeeds in splitting the system into an idealized and a deviatoric representation. The deviatoric system evaluates the response of isolated regions on the model where nonlinear or damage features are present. This is naturally coupled with the idealized system through the interface forces, allowing the system to capture the monolithic response under this additional forcing, neglecting the presence of localized features. The respective governing equations are reformulated to reflect this decomposition, and projection-based reduction driven by POD is applied separately to each set of equations. This allows coupling a physics-based reduction framework with a substructuring strategy, which, in turn, derives the proposed Component-Oriented Reduction (COR-ROM) approach and its hyper-reduced variation termed HpCOR-ROM.

The advantages of the proposed approach are illustrated on a toy case study of a four-story shear frame with multiple nonlinear regions driven by Bouc-Wen type hysteresis and further verified on a three-dimensional, large-scale case study of a kingpin connection, which is jointed via a welded region that exhibits material plasticity. Without making any problem-specific assumptions, the proposed COR-ROM delivered a robust and efficient performance in

Table 6 ROMs performance on capturing the time history responses $\boldsymbol{W}, \boldsymbol{Z}$ in the kingpin and welding regions, respectively. The reproduction of the stresses in the FOM is also evaluated

	Average error		Maximum error	
	Z_{error} (%)	W_{error} (%)	Z_{error} (%)	W_{error} (%)
Iso-ROM	0.14	<< 1	0.47	<< 1
COR-ROM	0.87	0.22	1.47	0.71
HpCOR-ROM	2.65	0.74	3.43	1.06
	Avg. σ_{error} (%)	Max. σ_{error} (%)	Weld elements	Comp. time (s)
Iso-ROM	0.85	1.52	11543	2645
COR-ROM	8.12	11.21	11543	1360
HpCOR-ROM	13.39	16.13	891	557

capturing response measures of the FOM behavior, like displacements, accelerations, and stresses under varying operational parameters.

In addition, the proposed COR-ROM outperformed system-oriented global reduction schemes while still providing accelerated model evaluations, thus highlighting the potential a component-oriented reduction treatment can offer.

Finally, due to the component-oriented nature of the approach, the implemented ROMs are beneficial for intricate systems comprising multiple components that may exhibit localized nonlinear features. The framework utilizes individual component modes to capture localized effects while additionally relying on reduction modes of a global nature to reproduce dynamic phenomena taking place on a system scale. As a result, in the case of extended instead of localized features, the accuracy of the approach may not be compromised. Still, its computational efficiency will strongly rely on the relative size of the isolated region.

Regarding the limitations of the current work and potential extensions, the decomposition technique as presented requires that the nonlinearities are isolated, with the region known a priori. While somewhat restrictive, this is nonetheless a common framework for structural systems, where hot-spot locations are often known a priori. Nevertheless, the proposed approach can be extended to first identify the domain(s) of nonlinear features and, in turn, perform the proposed decomposition automatically, assuming a suitable extent for the isolated region. In addition, the derived COR-ROM is most appropriate for systems with isolated nonlinearities, as the employed decomposition technique relies on the inherent assumption that the system comprises non-zero tangent stiffness in all model regions. In the presence of regions with zero tangent stiffness, numerical remedies can be implemented to avoid singularities or bad conditioning, e.g., artificial (non-zero) terms can be added to the stiffness matrix $\tilde{\boldsymbol{K}}$ and subsequently subtracted from the isolated nonlinearities term $\boldsymbol{G}_\star$ in Eq. (2). However, a robust regime would require a more refined approach, which is left for future work. The same applies to mitigating the curse of dimensionality during the training process, as additional adaptation is needed to optimize the selection of the training samples, primarily when many parametric traits are modeled.

Author contributions All authors contributed to the study's conception and design. Material preparation, data collection, and analysis were performed by Konstantinos Vlachas and D. Dane Quinn. The first draft of the manuscript was written by Konstantinos Vlachas, and all authors commented on previous versions. All authors read and approved the final manuscript.

Funding Open access funding provided by Swiss Federal Institute of Technology Zurich This research has been funded by the Sandia National Laboratories. Sandia National Laboratories is a multimission laboratory managed and operated by National Technology and Engineering Solutions of Sandia, LLC, a wholly owned subsidiary of Honeywell International Inc., for the US Department of Energy's National Nuclear Security Administration under contract DE-NA0003525. This paper describes objective technical results and analysis. Any subjective views or opinions that might be expressed in the paper do not necessarily represent the views of the US Department of Energy or the United States Government.

Data Availability The code that supports the findings for the four-story shear frame case study is openly available at [61].

The data supporting the rest of the results are available from the corresponding author upon reasonable request.

Declarations

Conflict of interest The authors have no relevant financial or non-financial interests to disclose.

Open Access This article is licensed under a Creative Commons Attribution 4.0 International License, which permits use, sharing, adaptation, distribution and reproduction in any medium or format, as long as you give appropriate credit to the original author(s) and the source, provide a link to the Creative Commons licence, and indicate if changes were made. The images or other third party material in this article are included in the article's Creative Commons licence, unless indicated otherwise in a credit line to the material. If material is not included in the article's Creative Commons licence and your intended use is not permitted by statutory regulation or exceeds the permitted use, you will need to obtain permission directly from the copyright holder. To view a copy of this licence, visit http://creativecommons.org/licenses/by/4.0/.

References

1. Weng, S., Zhu, H., Xia, Y., Li, J., Tian, W.: A review on dynamic substructuring methods for model updating and damage detection of large-scale structures. Adv. Struct. Eng. **23**(3), 584–600 (2020)
2. Tchemodanova, S.P., Sanayei, M., Moaveni, B., Tatsis, K., Chatzi, E.: Strain predictions at unmeasured locations of a substructure using sparse response-only vibration measurements. J. Civ. Struct. Heal. Monit. **11**(4), 1113–1136 (2021)
3. Chinesta, F., Cueto, E., Abisset-Chavanne, E., Duval, J.L., El Khaldi, F.: Virtual, digital and hybrid twins: a new paradigm in data-based engineering and engineered data. Arch. Comput. Methods Eng. **27**(1), 105–134 (2020)
4. Thelen, A., Zhang, X., Fink, O., Lu, Y., Ghosh, S., Youn, B.D., et al.: A comprehensive review of digital twin-part 1: modeling and twinning enabling technologies. Struct. Multidiscip. Optim. **65**(12), 354 (2022)
5. Tatsis, K.E., Agathos, K., Chatzi, E., Dertimanis, V.K.: A hierarchical output-only Bayesian approach for online vibration-based crack detection using parametric reduced-order models. Mech. Syst. Signal Process. **167**, 108558 (2022)
6. Allen, M.S., Rixen, D., Van der Seijs, M., Tiso, P., Abrahamsson, T., Mayes, R.L.: Substructuring in Engineering Dynamics. Springer, USA (2020)
7. Tatsis, K., Dertimanis, V., Papadimitriou, C., Lourens, E., Chatzi, E.: A general substructure-based framework for input-state estimation using limited output measurements. Mech. Syst. Signal Process. **150**, 107223 (2021)
8. de Klerk, D., Rixen, D.J., Voormeeren, S.: General framework for dynamic substructuring: history, review and classification of techniques. AIAA J. **46**(5), 1169–1181 (2008)
9. Gruber, F.M., Rixen, D.J.: Evaluation of substructure reduction techniques with fixed and free interfaces. Strojniški vestnik-J. Mech. Eng. **62**(7–8), 452–462 (2016)
10. Gruber, FM., Rixen, D.: Comparison of Craig-Bampton approaches for systems with arbitrary viscous damping in dynamic substructuring. In: Dynamics of Coupled Structures, Volume 4. Springer; p. 35–49 (2018)
11. Krattiger, D., Wu, L., Zacharczuk, M., Buck, M., Kuether, R.J., Allen, M.S., et al.: Interface reduction for Hurty/Craig-Bampton substructured models: review and improvements. Mech. Syst. Signal Process. **114**, 579–603 (2019)
12. Géradin, M., Rixen, D.J.: A fresh look at the dynamics of a flexible body application to substructuring for flexible multibody dynamics. Int. J. Numer. Meth. Eng. **122**(14), 3525–3582 (2021)
13. Insam, C., Kist, A., Schwalm, H., Rixen, D.J.: Robust and high fidelity real-time hybrid substructuring. Mech. Syst. Signal Process. **157**, 107720 (2021)
14. Wagg, D., Worden, K., Barthorpe, R., Gardner, P.: Digital twins: state-of-the-art and future directions for modeling and simulation in engineering dynamics applications. ASCE-ASME J. Risk Uncert in Engrg Syst. Part B Mech. Engrg. **6**(3), 030901 (2020)
15. Benner, P., Ohlberger, M., Cohen, A., Willcox, K.: Model reduction and approximation: theory and algorithms. SIAM (2017)
16. Swischuk, R., Mainini, L., Peherstorfer, B., Willcox, K.: Projection-based model reduction: formulations for physics-based machine learning. Comput Fluids. **179**, 704–717 (2019)
17. Mereles, A., Alves, DS., Cavalca, KL.: Model reduction of rotor-foundation systems using the approximate invariant manifold method. Nonlinear Dynamics. p. 1–26 (2023)
18. Gruber, F.M., Rixen, D.J.: Dual Craig-Bampton component mode synthesis method for model order reduction of non-classically damped linear systems. Mech. Syst. Signal Process. **111**, 678–698 (2018)
19. Worden, K., Cross, E.J., Gardner, P., Barthorpe, R.J., Wagg, D.J.: On Digital Twins. Mirrors and Virtualisations. in Springer International Publishing, Model Validation and Uncertainty Quantification (2019)
20. Hong, S.K., Epureanu, B.I., Castanier, M.P.: Next-generation parametric reduced-order models. Mech. Syst. Signal Process. **37**(1–2), 403–421 (2013)
21. Hong, SK., Castanier, MP., Epureanu, BI.: Parametric reduced order models for predicting the nonlinear vibration response of cracked structures with uncertainty. In: Sensors and Smart Structures Technologies for Civil, Mechanical, and Aerospace Systems 2009. vol. 7292. International Society for Optics and Photonics; p. 72921E (2009)
22. Lee, J., Cho, M.: An interpolation-based parametric reduced order model combined with component mode synthesis. Comput. Methods Appl. Mech. Eng. **319**, 258–286 (2017)
23. Lee, J.: A dynamic substructuring-based parametric reduced-order model considering the interpolation of free-interface substructural modes. J. Mech. Sci. Technol. **32**(12), 5831–5838 (2018)
24. Lee, J.: A parametric reduced-order model using substructural mode selections and interpolation. Comput. Struct. **212**, 199–214 (2019)
25. Liu, Y., Li, H., Li, Y., Du, H.: A component-based parametric reduced-order modeling method combined with substructural matrix interpolation and automatic sampling. Shock and Vib. **2019**(2), 1–14 (2019)

26. Kuether, R.J., Allen, M.S., Hollkamp, J.J.: Modal substructuring of geometrically nonlinear finite element models with interface reduction. AIAA J. **55**(5), 1695–1706 (2017)
27. Simpson, T., Giagopoulos, D., Dertimanis, V., Chatzi, E.: On dynamic substructuring of systems with localised nonlinearities. In: Dynamic Substructures. vol. 4. Springer; p. 105–116 (2020)
28. Roettgen, D., Seeger, B., Tai, WC., Baek, S., Dossogne, T., Allen, M., et al. A comparison of reduced order modeling techniques used in dynamic substructuring. In: Dynamics of Coupled Structures, Volume 4: Proceedings of the 34th IMAC, A Conference and Exposition on Structural Dynamics 2016. Springer; p. 511–528 (2016)
29. Kuether, R.J., Allen, M.S., Hollkamp, J.J.: Modal substructuring of geometrically nonlinear finite-element models. AIAA J. **54**(2), 691–702 (2016)
30. Latini, F., Brunetti, J., D'Ambrogio, W., Allen, M.S., Fregolent, A.: Nonlinear substructuring in the modal domain: numerical validation and experimental verification in presence of localized nonlinearities. Nonlinear Dyn. **104**, 1043–1067 (2021)
31. Wu, L., Tiso, P.: Nonlinear model order reduction for flexible multibody dynamics: a modal derivatives approach. Multibody Sys.Dyn. **36**(4), 405–425 (2016)
32. Wu, L., Tiso, P., Tatsis, K., Chatzi, E., van Keulen, F.: A modal derivatives enhanced Rubin substructuring method for geometrically nonlinear multibody systems. Multibody Sys.Dyn. **45**(1), 57–85 (2019)
33. Witteveen, W., Pichler, F.: Efficient model order reduction for the nonlinear dynamics of jointed structures by the use of trial vector derivatives. In: Dynamics of Coupled Structures, Volume 1. Springer; p. 147–155 (2014)
34. Allen, M.S., Rixen, D., van der Seijs, M., Tiso, P., Abrahamsson, T., Mayes, R.L., et al.: Model reduction concepts and substructuring approaches for nonlinear systems. Substructur. Eng. Dyn. Emerg. Numer. Exper. Techn. **2020**, 233–267 (2020)
35. Touzé, C., Vizzaccaro, A., Thomas, O.: Model order reduction methods for geometrically nonlinear structures: a review of nonlinear techniques. Nonlinear Dyn. **105**(2), 1141–1190 (2021)
36. Simpson, T., Dervilis, N., Chatzi, E.: On the use of nonlinear normal modes for nonlinear reduced order modelling. arXiv preprint arXiv:2007.00466. (2020)
37. Peeters, M., Viguié, R., Sérandour, G., Kerschen, G., Golinval, J.C.: Nonlinear normal modes, Part II: Toward a practical computation using numerical continuation techniques. Mech. Syst. Signal Process. **23**(1), 195–216 (2009)
38. Joannin, C., Chouvion, B., Thouverez, F., Ousty, J.P., Mbaye, M.: A nonlinear component mode synthesis method for the computation of steady-state vibrations in non-conservative systems. Mech. Syst. Signal Process. **83**, 75–92 (2017)
39. Kerschen, G.: Computation of nonlinear normal modes through shooting and pseudo-arclength computation. Modal Analysis of Nonlinear Mechanical Systems. p. 215–250 (2014)
40. Renson, L., Kerschen, G., Cochelin, B.: Numerical computation of nonlinear normal modes in mechanical engineering. J. Sound Vib. **364**, 177–206 (2016)
41. Kuether, R.J., Renson, L., Detroux, T., Grappasonni, C., Kerschen, G., Allen, M.S.: Nonlinear normal modes, modal interactions and isolated resonance curves. J. Sound Vib. **351**, 299–310 (2015)
42. Falco, M., Mahdiabadi, MK., Rixen, DJ.: Nonlinear substructuring using fixed interface nonlinear normal modes. In: Dynamics of Coupled Structures, Volume 4. Springer; p. 205–213 (2017)
43. Huang, X.R., Jézéquel, L., Besset, S., Li, L., Sauvage, O.: Nonlinear modal synthesis for analyzing structures with a frictional interface using a generalized Masing model. J. Sound Vib. **434**, 166–191 (2018)
44. Joannin, C., Thouverez, F., Chouvion, B.: Reduced-order modelling using nonlinear modes and triple nonlinear modal synthesis. Comput. Struct. **203**, 18–33 (2018)
45. Kerschen, G., Jc, Golinval, Vakakis, A.F., Bergman, L.A.: The method of proper orthogonal decomposition for dynamical characterization and order reduction of mechanical systems: an overview. Nonlinear Dyn. **41**(1–3), 147–169 (2005)
46. Simpson, T., Dervilis, N., Chatzi, E.: Machine learning approach to model order reduction of nonlinear systems via autoencoder and LSTM networks. J. Eng. Mech. **147**(10), 04021061 (2021)
47. Vlachas, K., Tatsis, K., Agathos, K., Brink, A.R., Chatzi, E.: A local basis approximation approach for nonlinear parametric model order reduction. J. Sound Vib. **502**, 116055 (2021)
48. Quinn, D.D.: Modal analysis of jointed structures. J. Sound Vib. **331**(1), 81–93 (2012)
49. Quinn, D.D., Brink, A.R.: Global system reduction order modeling for localized feature inclusion. J. Vib. Acoust. **143**(4), 041006 (2021)
50. Najera-Flores, D., Quinn, DD., Garland, A., Vlachas, K., Chatzi, E., Todd, M.: A machine learning framework for accurate prediction of structural dynamics for systems with isolated nonlinearities; Manuscript submitted for publication (2023)
51. Holzwarth, P., Eberhard, P.: SVD-based improvements for component mode synthesis in elastic multibody systems. Eur. J. Mech.-A/Solids. **49**, 408–418 (2015)
52. Im, S., Kim, E., Cho, M.: Reduction process based on proper orthogonal decomposition for dual formulation of dynamic substructures. Comput. Mech. **64**(5), 1237–1257 (2019)
53. Jin, Y., Lu, K., Huang, C., Hou, L., Chen, Y.: Nonlinear dynamic analysis of a complex dual rotor-bearing system based on a novel model reduction method. Appl. Math. Model. **75**, 553–571 (2019)
54. Agathos, K., Bordas, S.P., Chatzi, E.: Parametrized reduced order modeling for cracked solids. Int. J. Numer. Meth. Eng. **121**(20), 4537–4565 (2020)
55. Farhat, C., Avery, P., Chapman, T., Cortial, J.: Dimensional reduction of nonlinear finite element dynamic models with finite rotations and energy-based mesh sampling and weighting for computational efficiency. Int. J. Numer. Meth. Eng. **98**(9), 625–662 (2014)
56. Ghavamian, F., Tiso, P., Simone, A.: POD-DEIM model order reduction for strain-softening viscoplasticity. Comput. Methods Appl. Mech. Eng. **317**, 458–479 (2017)
57. Jain, S., Tiso, P.: Hyper-reduction over nonlinear manifolds for large nonlinear mechanical systems. J. Comput. Nonlinear Dyn. **14**(8), 081008 (2019)

58. Hesthaven, J.S., Stamm, B., Zhang, S.: Efficient greedy algorithms for high-dimensional parameter spaces with applications to empirical interpolation and reduced basis methods. ESAIM Math. Modell. Numer. Anal. **48**(1), 259–283 (2014)
59. Amsallem, D., Farhat, C.: An online method for interpolating linear parametric reduced-order models. SIAM J. Sci. Comput. **33**(5), 2169–2198 (2011)
60. Vlachas, K., Tatsis, K., Agathos, K., Brink, AR., Quinn, DD., Chatzi, E.: On the Coupling of Reduced Order Modeling with Substructuring of Structural Systems with Component Nonlinearities. In: Dynamic Substructures, Volume 4. Springer; p. 35–43 (2022)
61. Vlachas, K., Agathos, K., Tatsis, KE., Brink, AR., Chatzi, E.: Two-story frame with Bouc-Wen hysteretic links as a multi-degree of freedom nonlinear response simulator. In: 5th Workshop on Nonlinear System Identification Benchmarks (2021); p. 6 (2021)
62. Vlachas, K., Tatsis, K., Agathos, K., Brink, AR., Chatzi, E.: Two-story frame with Bouc-Wen hysteretic links as a multi-degree of freedom nonlinear response simulator. (2021) https://doi.org/10.5281/zenodo.4742248
63. Amsallem, D., Haasdonk, B.: PEBL-ROM: projection-error based local reduced-order models. Adv. Model. Simul. Eng. Sci. **3**, 1–25 (2016)
64. Quarteroni, A., Rozza, G., et al. Reduced order methods for modeling and computational reduction. vol. 9. Springer; (2014)
65. Haasdonk, B., Dihlmann, M., Ohlberger, M.: A training set and multiple bases generation approach for parameterized model reduction based on adaptive grids in parameter space. Math. Comput. Model. Dyn. Syst. **17**(4), 423–442 (2011)
66. Rozza, G., Huynh, D.B.P., Patera, A.T.: Reduced basis approximation and a posteriori error estimation for affinely parametrized elliptic coercive partial differential equations. Arch. Comput. Methods Eng. **15**(3), 229–275 (2008)
67. Rozza, G., Huynh, D.P., Manzoni, A.: Reduced basis approximation and a posteriori error estimation for Stokes flows in parametrized geometries: roles of the inf-sup stability constants. Numer. Math. **125**(1), 115–152 (2013)
68. Allemang, R.J.: The modal assurance criterion-twenty years of use and abuse. Sound and Vibration. **37**(8), 14–23 (2003)
69. MacQueen J, et al. Some methods for classification and analysis of multivariate observations. In: Proceedings of the fifth Berkeley symposium on mathematical statistics and probability. vol. 1. Oakland, CA, USA; p. 281–297 (1967)
70. Vlachas, K., Tatsis, K., Agathos, K., Brink, AR., Quinn, DD., Chatzi, E.: Parametric model order reduction for localized nonlinear feature inclusion. In: Advances in Nonlinear Dynamics: Proceedings of the Second International Nonlinear Dynamics Conference (NODYCON 2021), Volume 1. Springer; p. 373–383 (2021)
71. Paul-Dubois-Taine, A., Amsallem, D.: An adaptive and efficient greedy procedure for the optimal training of parametric reduced-order models. Int. J. Numer. Meth. Eng. **102**(5), 1262–1292 (2015)
72. Urban, K., Volkwein, S., Zeeb, O.: Greedy sampling using nonlinear optimization. Reduced Order Methods for modeling and computational reduction. p. 137–157 (2014)
73. Jiang, J., Chen, Y., Narayan, A.: Offline-enhanced reduced basis method through adaptive construction of the surrogate training set. J. Sci. Comput. **73**, 853–875 (2017)
74. Peherstorfer, B., Butnaru, D., Willcox, K., Bungartz, H.J.: Localized discrete empirical interpolation method. SIAM J. Sci. Comput. **36**(1), A168–A192 (2014)
75. Farhat, C., Chapman, T., Avery, P.: Structure-preserving, stability, and accuracy properties of the energy-conserving sampling and weighting method for the hyper reduction of nonlinear finite element dynamic models. Int. J. Numer. Meth. Eng. **102**(5), 1077–1110 (2015)
76. Agathos, K., Tatsis, K.E., Vlachas, K., Chatzi, E.: Parametric reduced order models for output-only vibration-based crack detection in shell structures. Mech. Syst. Signal Process. **162**, 108051 (2022)
77. Peharz, R., Pernkopf, F.: Sparse nonnegative matrix factorization with ℓ^0-constraints. Neurocomputing **80**, 38–46 (2012)
78. Mathis, A.T., Balaji, N.N., Kuether, R.J., Brink, A.R., Brake, M.R., Quinn, D.D.: A review of damping models for structures with mechanical joints. Appl. Mech. Rev. **72**(4), 040802 (2020)
79. Ismail, M., Ikhouane, F., Rodellar, J.: The hysteresis Bouc-Wen model, a survey. Arch. Comput. Methods Eng. **16**(2), 161–188 (2009)
80. Lacarbonara, W.: Nonlinear structural mechanics: theory, dynamical phenomena and modeling. Springer Science & Business Media, UK (2013)
81. Simpson, T., Vlachas, K., Garland, A., Dervilis, N., Chatzi, E.: VpROM: A novelVariational AutoEncoder-boosted Reduced Order Model for the treatment of parametric dependencies in nonlinear systems. arXiv preprint arXiv:2304.12437. (2023)
82. Vlachas, K., Tatsis, K., Agathos, K., Brink, AR., Chatzi, E.: A physics-based, local POD basis approach for multi-parametric reduced order models. In: International Conference on Noise and Vibration Engineering (ISMA 2020) in conjunction with the 8th International Conference on Uncertainty in Structural Dynamics (USD 2020). ETH Zurich, Environmental and Geomatic Engineering; p. 228 (2020)
83. Spiridonakos, M.D., Chatzi, E.N.: Metamodeling of dynamic nonlinear structural systems through polynomial chaos NARX models. Comput. Struct. **157**, 99–113 (2015)
84. Rezaeian, S., Der Kiureghian, A.: Simulation of synthetic ground motions for specified earthquake and site characteristics. Earthq Eng. Struct. Dyn. **39**(10), 1155–1180 (2010)
85. Spiridonakos, M., Vlachas, K., Chatzi, E.: Parametric representation of synthetic earthquakes; (2022). Available from: https://github.com/KosVla/ParametricSyntheticEarthquakes
86. Ancheta, TD., Darragh, RB., Stewart, JP., Seyhan, E., Silva, WJ., Chiou, BS., et al. Pacific earthquake engineering research center; (2013). Available from: https://ngawest2.berkeley.edu/

Publisher's Note Springer Nature remains neutral with regard to jurisdictional claims in published maps and institutional affiliations.